TECHNICAL OPERATIONS RESEARCH

AD 601 719

EXPERIMENTAL DETERMINATION OF THE WALL-SCATTERED RADIATION FUNCTION $G_s(\omega)$

By

James L. Jones
John F. Batter

Report No. TO-B 63-88
Contract No. OCD-OS-62-14

December, 1963

Submitted to

Office of Civil Defense
Department of Defense
Washington, D. C.

tech ops

DDC AVAILABILITY

Qualified requestors may obtain copies of this report from the Defense Documentation Center, Cameron Station, Alexandria, Virginia.

tech ops

TECHNICAL OPERATIONS RESEARCH

EXPERIMENTAL DETERMINATION OF THE WALL-SCATTERED RADIATION FUNCTION $G_s(\omega)$

By

James L. Jones
John F. Batter

Report No. TO-B 63-88

December, 1963

OCD REVIEW NOTICE

This report has been reviewed in the Office of Civil Defense and approved for publication. Approval does not signify that the contents necessarily reflect the views and policies of the Office of Civil Defense.

Prepared for

Office of Civil Defense
Department of Defense
Under
Contract No. OCD-OS-62-14
Subtask 1111A

Burlington, Massachusetts

ACKNOWLEDGMENTS

The authors are indebted to Mrs. Nancy-Ruth York, Mr. Robert MacNeil, and Mr. Sheldon Hunt for the skill and dedication shown in performing these experiments, and to Mr. Matthew Barrett for discussions and review of the analysis.

ABSTRACT

In this report we investigated the variation of dose rate with solid angle fraction in structures of simple geometries and compared the experimentally determined infinite field dose rate with that calculated using the formula

$$D^{\infty} = B_w \quad 0.5 S_w E \left[S_a(\omega_u) - S_a(\omega_{u'}) \right] + 0.088(1 - S_w) \left[S_a(\omega_u) - S_a(\omega_{u'}) \right] .$$

The geometry factor for skyshine radiation $S_a(\omega)$ was taken from Figure B37 of "Structure Shielding Against Fallout Radiation from Nuclear Weapons" by L. V. Spencer and was applied to wall-scattered radiation as described in "An Engineering Method for Calculating Protection Afforded by Structures Against Fallout Radiation" by C. Eisenhauer. The factors $B_w(X_e)$, E, and $S_w(X_e)$ were taken from the Engineering Manual "Design and Review of Structures for Protection from Fallout Gamma Radiation."

Except for the thinnest walls, the values of experimental and calculated dose rates were within 20%. This was greater than the estimated experimental error, and the difference followed a pattern that suggests a definite discrepancy between experiment and calculation. The same pattern of discrepancies was found in a direct comparison of experimental and theoretical values of $S_a(\omega)$.

TABLE OF CONTENTS

LIST OF ILLUSTRATIONS

LIST OF TABLES

LIST OF TABLES (Cont'd.)

CHAPTER 1

INTRODUCTION

The prediction of dose rates to be expected in a radiation shelter due to external sources presents a problem far more complicated than that of determining the attenuation of a narrow, collimated beam of radiation traversing a thickness of material and being measured by a collimated detector. The dose rate in a shelter, besides the narrow beam contribution of direct radiation, will include secondaries scattered through all angles and often of comparable intensity.

During recent years this aspect of radiation shielding has been intensively investigated with particular emphasis on applications to shelters. Of particular importance has been a series of machine computations of gamma ray scattering and attenuation functions prepared and compiled by Dr. L. V. Spencer[1] using the moment method and Monte Carlo techniques based on fundamental cross-section data. Computations of the angular distribution of scattered radiation at various distances from point and plane sources yielded twenty-five graphs from which flexible, self-consistent methods of analysis were derived by Mr. Charles Eisenhauer and Mr. L. N. FitzSimons working in conjunction with Dr. Spencer. These curves, computed for Co-60, Cs-137, and 1.12-hr fallout radiation, have been published in the so-called Engineering Manual[2], which is designed to assist architects and engineers in the design of structures for fallout protection.

To date, these methods have been experimentally evaluated only by whole building exposures — structures so complicated as to yield little basic information, though providing significant confirmation of the general applicability of the method. The basic premises of this important field, therefore, have not been tested experimentally. This experiment was planned to test the premises by using the simplest possible structure, thus reducing the measured dose rate to a function solely of the subtended solid angle and the thickness of the scattering walls.

A cylindrical shell at the center of a circular field was used to provide this simplicity, with the additional advantage of circular symmetry, making possible the replacement of the plane source by a succession of point sources along one radius. Wall thickness was changed by adding successive half-cylinders, and solid angle

was changed by placing the detector at different depths in a hole beneath the cylinder. Below-surface positions were necessary to eliminate direct radiation. The information derived from this experiment about the variation of dose rate with solid angle for a given cylinder thickness could then be compared with calculations based on the Engineering Manual and Spencer's Monograph. In the second part of the experiment, the cylinder was replaced by a wall of 1-in. thick steel, 6 ft by 12 ft, to test the possible influence of structure configuration on the dose rate.

The experiment is described in detail in Chapter 2. The basic data are presented in Chapter 3 and are analyzed in Chapter 4. Chapter 5 contains the conclusions derived from the experiment. An experimental curve for $S_a(\omega)$ is derived in Chapter 6 and is compared with the theory.

CHAPTER 2

DESCRIPTION OF EXPERIMENT

The primary purpose of this experiment was to investigate the validity of the assumptions made by Eisenhauer and Spencer in deriving the curve of $G_s(\omega)$, defined as a scattering function such that $D^{\infty} = \alpha(X_e)\left[G_s(\omega_u) + G_s(\omega_\ell)\right]$, in which ω_u is that fraction of the upper hemisphere not subtended by the scattering surface, and ω_ℓ is that fraction of the lower hemisphere not subtended by the scattering surface. This requires experimental knowledge of the variation of dose rate with solid angle with minimal structural or radiation complications and of the effect of wall thickness and structure shape on the dose rate.

OUTLINE OF EXPERIMENT

To achieve a direct dependence on solid angle, the detector was placed on the axis of a steel cylinder subtending solid angle $\omega = 1 - \cos O$, where O is the angle between the cylinder axis and a line from the detector to the upper (ω_u) or lower ($\omega_{u'}$) edge of the cylinder (Figure 1). The dose rate could then be measured at different detector positions along the axis, expressed in terms of ω, and a comparison made with $G_s(\omega)$. However, the detector had to be placed below the level of the contaminated plane to eliminate direct radiation, giving an expression $D^{\infty} = \alpha\left[G_s(\omega_u) - G_s(\omega_{u'})\right]$. The curve of $G_s(\omega)$ was derived from Spencer's $S_a(d,\omega)$ by the relation $G_s = 0.5\left[1 - S_a(d,\omega)\right]$. Since the $G_s(\omega)$ curve in the Engineering Manual refers to fallout radiation, calculations were based on the $S_a(d,\omega)$ curve in Spencer's monograph for Co-60 radiation using the formula

$$D^{\infty} = 0.5\,\alpha\left[S_a(\omega_{u'}) - S_a(\omega_u)\right].$$

Possible dependence of $G_s(\omega)$ on wall thickness was investigated by varying the mass thickness of the cylinder; its dependence on structure shape was determined by replacing the cylinder with a rectangular wall.

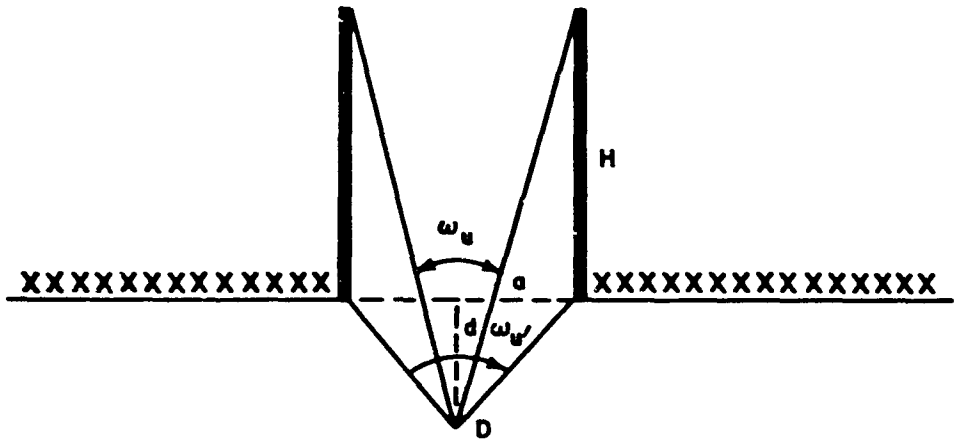

$$\omega_u = 1 - \frac{d+H}{\sqrt{(d+H)^2 + a^2}}$$

$$\omega_{u'} = 1 - \frac{d}{\sqrt{d^2 + a^2}}$$

Figure 1. Solid Angles Subtended by Upper and Lower Limits of the Cylinder at Detector Position D

However, the majority of the experiments were performed on the cylinder to take advantage of its symmetry, which permitted a point source to represent a ring source in the following way. If a source qS_o is placed a distance r from a detector, the response will be

$$D_m = \frac{qS_o}{r^2} .$$

If qS_o is considered a linear radiation density, then the total response at the center of a circle of such line charge is $2\pi r qS_o/r^2$, since the contribution from one element is equal to that from any other. If this circumferential source is thought to represent an annular ring of area $2\pi r dr$, then the ring contributes

$$dD = qS_o \cdot 2\pi r \frac{dr}{dr^2}$$

or

$$\frac{dD}{dr} = 2\pi r D_m$$

and the total field can be approximated by a summation of elements $2\pi r \Delta r D_m$, being represented by individual point sources a distance Δr apart along one radial line. Since $2\pi r D_m = D_{exp}$ is the basic datum, all measurements are expressed in this form and are normalized to a field strength of 1 curie/ft^2.

The same philosophy was followed in simulating the field for the rectangular wall except that the response would vary with the angle ϕ between the perpendicular to the plate and the source-detector line. The total response would then involve a summation over radius followed by a summation over the angle ϕ.

CHOICE OF MATERIAL

As Eisenhauer[3] points out, his curve for $G_s(\omega)$ is based on skyshine; i.e., radiation scattered by an atmospheric medium. Practically, a denser scattering material was experimentally necessary and generally desirable for shelter applications. The significant choices were iron and concrete, both of which are presumed to be reasonably equivalent to air as scatterers, on a mass thickness basis, since the absorption coefficients of the lighter elements are quite close together at the photon energies of Co-60 or 1.12-hr fallout (around 1 MeV). Concrete would have greater applicability in structural shielding, but iron is easier to shape into the desired form and, more important, is much freer of voids and inhomogeneities. Since Monte Carlo calculations[4] indicate there is little actual difference in the scattering response of the two materials (Table 1), iron was chosen for the structural material.

EXPERIMENTAL STRUCTURES

The basic cylinder was constructed of steel 1/2-in. thick, 5-ft high, and 2-ft in diameter. The height seemed to approximate an infinite cylinder closely enough, since even at the highest detector position ω_u was quite close to 0 (specifically 0.0188). This assumption was justified by varying the cylinder height and by observing the change of dose rate. The dose rate was close to its asymptotic value at a 5-ft height (Figure 2). Thickness could be increased by adding 1/2-in.-thick half cylinders,

TABLE 1

ROOF REDUCTION FACTORS COMPUTED BY THE MONTE CARLO METHOD FOR A 1.25 MeV PLANE ISOTROPIC SOURCE ON A BARRIER OF 30 g/cm^2 = 61.5 psf EFFECTIVE MASS THICKNESS

ω	Concrete	Iron
0.094	0.0073	0.0076
0.234	0.0170	0.0176
0.357	0.0245	0.0257
0.500	0.0316	0.0326
0.658	0.0360	0.0383
0.826	0.0391	0.0412
0.913	0.0418	0.0424
1.000	0.0419	0.0429

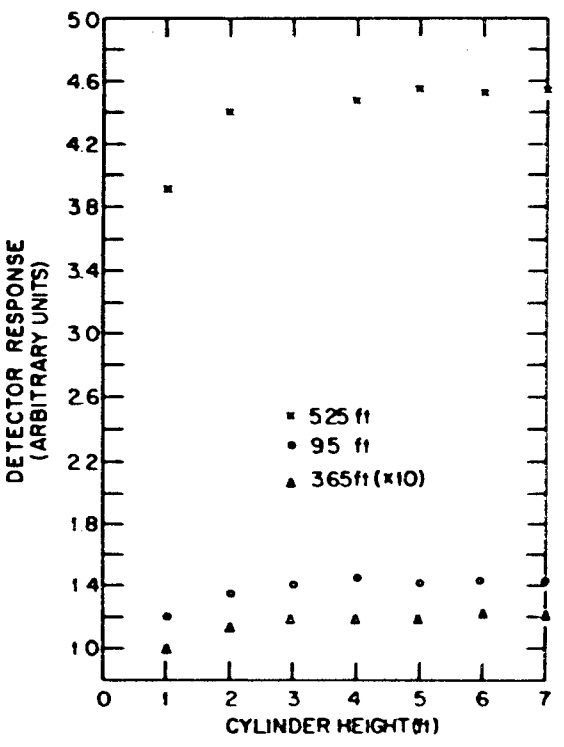

Figure 2. Variation of Detector Response with Cylinder Height for Various Source Positions (h = 3-in. depth)

shown in Figure 3, to the side of the cylinder facing the source. Experiments were conducted for four cases of effective mass thickness: (1) 1/2 in. or 18.6 psf; (2) 1 in. or 37.2 psf; (3) 1-1/2 in. or 55.9 psf; (4) 2 in. or 74.5 psf.

The rectangular wall was a 1-in.-thick steel slab 12 ft long by 6 ft high. At a detector position on a line 4 in. behind the wall, these dimensions gave solid angle subtended by the upper edge of the same order as that subtended in the cylinder. The assumption that this would give a response close to that of an infinite plate was tested and verified by adding a small extra plate (Figures 4 and 5).

The cylinder was placed over a hole of the same diameter and deep enough for

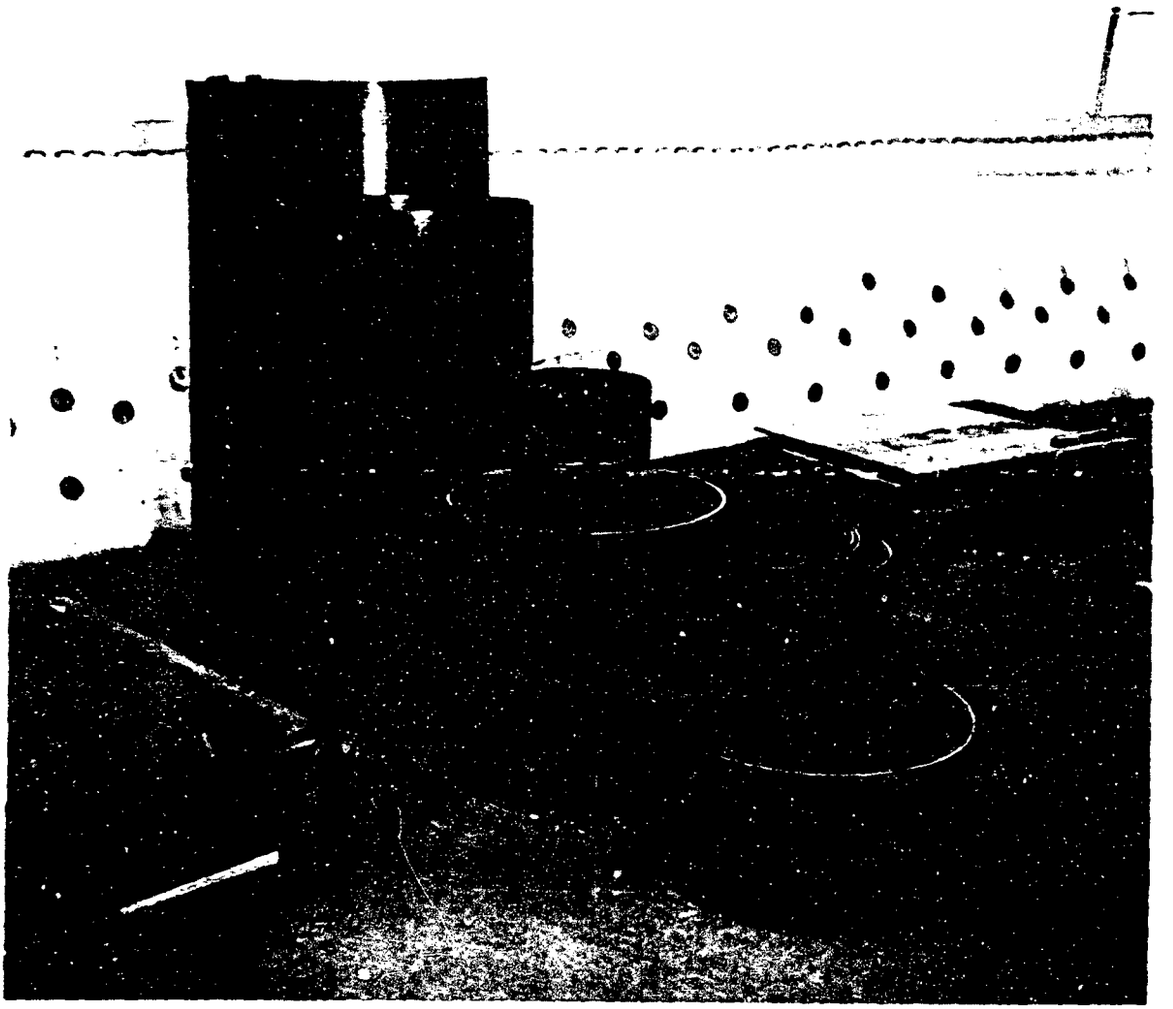

Figure 3. 1/2-in. Thick Cylinders and Semi-Cylinders Used in the Experiments

a 4-ft detector depth. The upper rim of the hole was lined with lead bricks to reduce edge effects. The rectangular wall was alongside a hole that only extended 3 ft on either side of the detector position, thus blocking some of the wall from the detector line-of-sight. The change this made in the solid angle of the wall at the detector was significant only for the deepest three positions (Table 2). The rim was lined with lead bricks, and a steel plate covered the portion of the hole behind the detector to reduce airscatter.

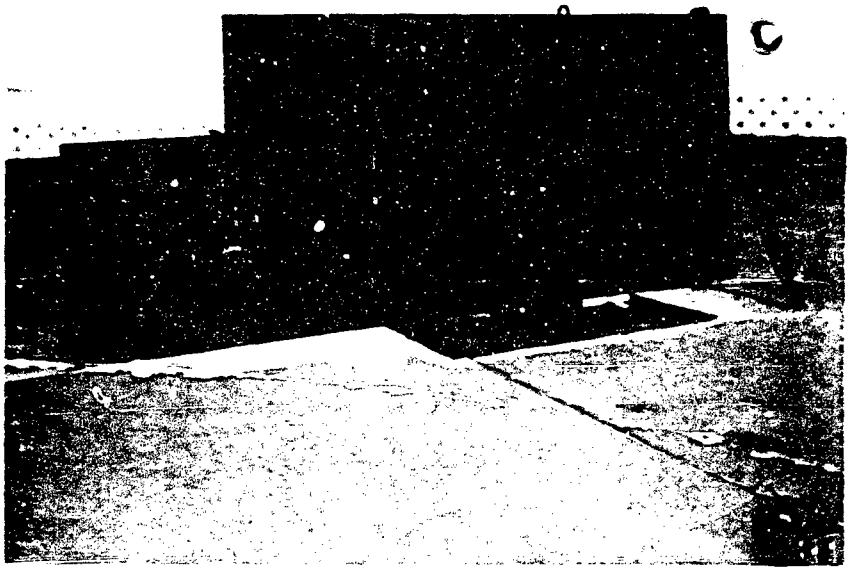

Figure 4. 1-in. Thick Rectangular Wall with Dosimeters in Position

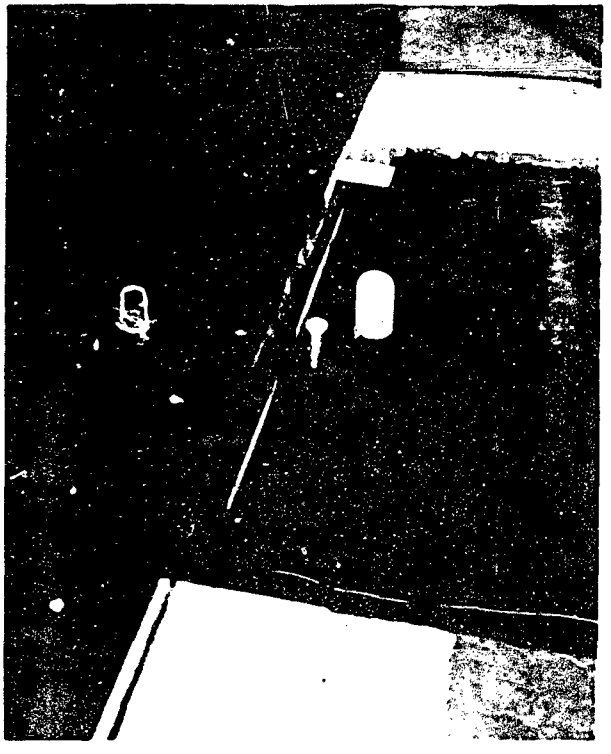

Figure 5. 1-in. Thick Rectangular Wall Showing Detector Pit and Ratemeter

TABLE 2

CHANGE IN SOLID ANGLE DUE TO LIMITED DETECTOR HOLE

Detector Depth L (in.)	ω_1	ω_2	$\frac{\omega_1}{\omega_2}$
36	0.0157	0.0181	0.867
24	0.0312	0.0335	0.931
12	0.0787	0.0805	0.978
6	0.1635	0.1637	0.999

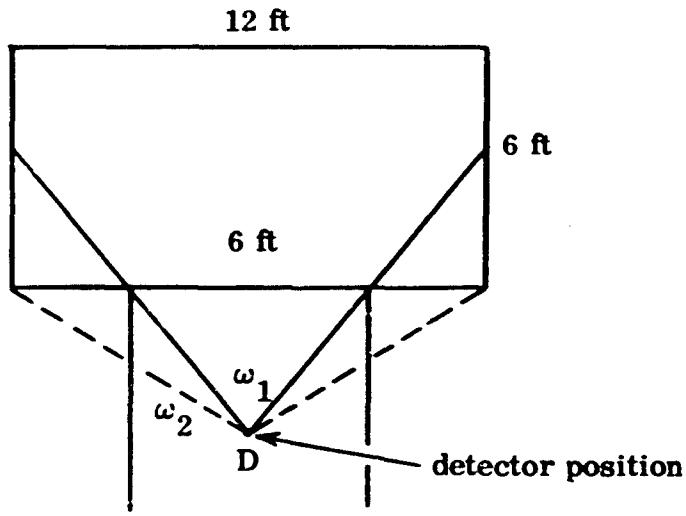

ω_1 = solid angle fraction subtended by the portion of the plate not hidden by the edges of the detector pit

ω_2 = solid angle fraction subtended by the entire plate.

POINT SOURCES

Point sources were placed manually at selected radial positions. Sources of approximately 20, 7, and 0.5 curies were used, depending on detector depth and source radius. The 0.5 curie source was rod-mounted and positioned by hand; the 7-curie and 20-curie sources were cranked into position through polyethylene tubing by a cable-type retrieval unit used for source positioning.

INSTRUMENTATION

At the deeper positions with smaller dose rates, the detector used was an ionization rate chamber removed from a standard Victoreen Model 592 Survey Meter. This chamber, with an approximate volume of 320 cm^3, was modified by increasing the resistance across the chamber by a factor of 6 to provide greater sensitivity. The chamber was enclosed in a polyethylene cover, 1/8-in. thick, to ensure that electrons caused by free-air ionization did not penetrate the chamber wall. The output of the chamber was fed to a solid-state amplifier — a specially designed low-noise, feedback type. To remove statistical fluctuations, the output of this amplifier was fed through a time-integrating circuit to a John Fluke digital null voltmeter. In this manner, the output of the chamber could be read to approximately two parts in a thousand with excellent reproducibility.

Near the surface, Victoreen Model 362 pocket dosimeters (200 mr) were used because of the appreciable vertical extent of the ratemeter. These were read with a portable charger-reader designed and constructed by Tech/Ops.

CALIBRATION

The ionization rate chamber used in the experiment was calibrated by exposing it to a standard Co-60 source previously calibrated by the National Bureau of Standards. Both chamber and source were placed on an essentially massless calibration bench approximately 9-1/4 ft above, and parallel to, the ground. Voltage readings of the chamber-amplifier output were taken at various source-to-detector distances ranging from 4 ft to 11 ft. These data were corrected for air attenuation, R^2 attenuation, and reflection of radiation from the ground to the detector. The resulting value of sensitivity obtained by extrapolating these calibration data to zero radius

for the detector-amplifier combination was 273 V output/r/hr. The detector response was determined to be essentially linear within 1/2 of 1% for voltage below 10 V. Thus, when taking data for this series of experiments, we vary the source strength to keep the maximum detector output below this value as much as possible.

A secondary calibration of the detector was performed by placing it within the hole and locating a small source of Co-60 in a fixed position relative to the detector immediately after the fundamental calibration was performed. This method of secondary calibration was repeated to evaluate the detector performance at the start and conclusion of each day's experimentation.

The calibration of dosimeters necessary to convert microampere readings from the charger-reader to dose values in milliroentgens was conducted outdoors to reduce scattering into the dosimeters. The dosimeters were carefully placed at heights above the ground that would minimize local effects of ground scattering without unduly complicating the procedure. All exposures were to Co-60 sources of known strength. Groups of identical dosimeters were placed a given distance from the source. Different exposures were obtained by varying the time of exposure. The dose was calculated based on an inverse square law behavior for source-dosimeter distance and no scattering, since the distances involved were small.

OPERATIONAL PROCEDURES

Personnel engaged in the experiment were equipped with 200 mr direct-reading dosimeters and film badges, and both the air-supported experimentation building and the control office were continuously monitored by Tech/Ops Model 492 "Gammalarms." In addition, during all manipulation of sources, two portable survey meters were used for personnel monitoring.

Dosimeters were accurately positioned at depths of 1, 2, 3, 4.5, and 6 in. on the axis of the cylinder. They were clipped to a plastic holder and exposed simultaneously. While one operator monitored from a safe distance, the other attached the point source to a 14-ft handling rod and positioned it, in the case of the 0.5-curie source, or fastened the end of the polyethylene tube at the proper position and cranked out the larger sources. After the exposure was completed, the source was replaced in its storage container, and the dosimeters read and replaced for the next

run. Readings were taken at radial positions of 1.75, 2.25, 2.75, 3.25, 3.75, 4.25, 4.75, 5.25, 5.75, 6.5, 7.5, 8.5, 11.0, 13.0, 15.0, 17.0, 19.0, 22.5, 27.5, 32.5, 37.5, and 42.5 ft, and extrapolations were made at 1.0, 9.5, and 45 ft.

The ratemeter was mounted on an aluminum rod and positioned by a pulley system. The same set of radial positions was measured at depths of 2.75, 4.25, 5.75, 8.75, 11.75, 17.75, 23.75, 35.75, and 47.75 in. The obscure depth settings resulted from an initial error of 0.25 in. in the ratemeter position. The solid angle subtended by the detector varied with its depth as $\omega = 1 - \cos \Theta$, where Θ is given by $\tan \Theta = a/h$; a is the radius of the cylinder; and h the detector depth.

For the rectangular walls, dosimeters were placed at depths of 1.0, 2.0, 4.0, and 6 in. and the ratemeters at depths of 4.0, 6.0, 12.0, 24.0, and 36 in. The source was placed at distances of 1.75, 3.75, 7.5, 22.5, and 42.5 ft, each radial line being repeated at 0, 20, 40, 55, 70, and 80 deg. The angular positions were chosen on the basis of a crude estimation of flux change with angle. Solid angle measurements were based on the inner edges of the structures.

CHAPTER 3

EXPERIMENTAL DATA

Tables 3, 4, 5, and 6 show measured values of $D_{exp} = 2\pi r D_m$ for effective mass thicknesses of 18.6, 37.2, 55.9, and 74.5 psf, respectively. Values at ρ = 1.00, 9.5, and 45 ft are extrapolated from curves of D_{exp} vs ρ. Table 7 gives D_{exp} for the rectangular wall. Dosimeter readings are at depths of 1 in., 2 in., 3 in., and the first listed at (4a) 4 in.; ratemeter readings are at 4(b), 6, 12, 24, and 36 in. Table 8 lists the value of solid angle fraction associated with each depth in the cylinder and wall. All values are normalized to a field strength of 1 curie/ft^2.

TABLE 3

DOSE RATE DATA IN 5-FT CYLINDER
(X_e = 18.6 psf) D_{exp} (mr/hr)/(curie/ft)

b(in.) / ρ(ft)	1.0	2.0	2.75	3.0	4.25	4.5	5.75	6.0	8.75	11.75	17.75	23.75	35.75	47.75
1.00	8.1	6.8	5.2	5.7	4.0	4.3	2.78	3.2	1.87	1.220	0.695	0.342	0.149	0.0780
1.75	5.2	4.4	3.59	3.65	3.59	2.94	2.24	2.28	1.38	0.923	0.464	0.265	0.111	0.0567
2.25	3.9	3.4	2.82	2.90	2.82	2.79	1.70	1.71	1.092	0.741	0.374	0.217	0.0940	0.0499
2.75	3.2	2.7	2.33	2.3	2.33	1.90	1.44	1.40	0.922	0.621	0.320	0.191	0.0833	0.0438
3.25	2.8	2.3	2.02	1.93	2.02	1.54	1.26	1.19	0.807	0.553	0.290	0 170	0.0745	0.0395
3.75	2.4	2.0	1.73	1.65	1.73	1.39	1.09	1.05	0.709	0.490	0.254	0.149	0.0650	0.0365
4.25	2.1	1.8	1.55	1.46	1.55	1.21	0.972	0.934	0.643	0.446	0.231	0.137	0.0625	0.0337
4.75	1.8	1.6	1.32	1.31	1.32	1.07	0.844	0.851	0.563	0.392	0.204	0.125	0.0574	0.0317
5.25	1.7	1.4	1.24	1.22	1.24	0.996	0.788	0.768	0.514	0.360	0.188	0.115	0.0537	0.0293
5.75	1.5	1.3	1.10	1.07	1.10	0.873	0.714	0.688	0.474	0.326	0.174	0.107	0.0505	0.0274
6.5	1.3	1.1	0.997	0.949	0.997	0.732	0.635	0.611	0.416	0.279	0.159	0.0971	0.0456	0.0249
7.5	1.2	1.0	0.845	0.854	0.845	0.687	0.554	0.548	0.371	0.257	0.139	0.0867	0.0409	0.0222
8.5	1.1	0.9	0.792	0.756	0.792	0.610	0.497	0.494	0.332	0.233	0.125	0.0773	0.0369	0.0203
9.5	0.96	0.8	0.70	0.66	0.70	0.54	0.438	0.42	0.295	0.211	0.117	0.0702	0.0339	0.0190
11.0	0.87	0.74	0.578	0.618	0.579	0.494	0.397	0.412	0.265	0.186	0.101	0.0632	0.030	0.0166
13.0	0.68	0.59	0.515	0.483	0.515	0.394	0.327	0.314	0.217	0.157	0.0833	0.0528	0.025	0.0139
15.0	0.60	0.51	0.435	0.431	0.435	0.348	0.290	0.278	0.193	0.136	0.0744	0.0468	0.0223	0.0124
17.0	0.53	0.46	0.399	0.385	0.398	0.317	0.238	0.253	0.170	0.121	0.0661	0.0410	0.0197	0.0108
19.0	0.47	0.40	0.349	0.336	0.349	0.271	0.225	0.212	0.152	0.108	0.0588	0.0365	0.0177	0.00968
22.5	0.38	0.33	0.301	0.272	0.3013	0.223	0.192	0.178	0.129	0.0919	0.0501	0.0313	0.0151	0.00849
27.5	0.31	0.27	0.238	0.226	0.238	0.178	0.149	0.143	0.103	0.0729	0.0407	0.0255	0.0121	0.00704
32.5	0.25	0.22	0.199	0.182	0.199	0.151	0.128	0.119	0.0848	0.0589	0.0334	0.0211	0.0104	0.00571
37.5	0.23	0.194	0.169	0.156	0.169	0.133	0.1099	0.1039	0.0733	0.0518	0.0289	0.0179	0.00898	0.00504
42.5	0.19	0.16	0.142	0.135	0.142	0.112	0.0914	0.0899	0.0649	0.0467	0.0263	0.0163	0.00784	0.00442
45.0	0.18	0.15	0.133	0.13	0.133	0.105	0.0827	0.084	0.060	0.0448	0.0299	0.0152	0.00739	0.00412

TABLE 4

DOSE RATE DATA IN 5-FT CYLINDER
(X_e = 37.2 psf) D_{exp} (mr/hr)/(curie/ft)

h(in.) / ρ(ft)	1.0	2.0	2.75	3.0	4.25	4.5	5.75	6.0	8.75	11.75	17.75	23.75	35.75	47.75
1.00	8.80	6.30	6.000	5.400	4.500	4.600	3.000	3.800	2.35	1.300	0.500	0.270	0.120	0.0520
1.75	4.99	4.29	4.119	3.678	3.098	2.002	2.321	2.189	1.383	0.883	0.393	0.216	0.0885	0.0445
2.25	3.94	3.28	2.90	2.664	2.429	2.220	1.898	1.720	1.117	0.705	0.326	0.183	0.0725	0.0380
2.75	3.10	2.62	2.479	2.127	1.977	1.719	1.510	1.313	0.904	0.601	0.284	0.161	0.0668	0.0345
3.25	2.81	2.33	2.05	1.965	1.636	1.554	1.321	1.188	0.776	0.518	0.249	0.142	0.0602	0.0303
3.75	2.29	1.87	1.861	1.590	1.462	1.263	1.150	0.889	0.696	0.453	0.221	0.126	0.0550	0.0283
4.25	2.02	1.74	1.652	1.551	1.267	1.175	1.019	0.893	0.622	0.415	0.202	0.115	0.0507	0.0261
4.75	1.93	1.56	1.46	1.368	1.165	0.990	0.920	0.802	0.563	0.342	0.183	0.104	0.0459	0.0242
5.25	1.72	1.50	1.335	1.276	1.011	1.008	0.817	0.772	0.515	0.335	0.170	0.0971	0.0432	0.0225
5.75	1.43	1.19	1.20	1.002	0.943	0.809	0.770	0.616	0.472	0.309	0.156	0.0903	0.0406	0.0213
6.5	1.36	1.16	1.052	0.969	0.812	0.755	0.661	0.579	0.408	0.276	0.140	0.0807	0.0364	0.0191
7.5	1.17	0.976	0.940	0.839	0.724	0.684	0.600	0.513	0.359	0.239	0.125	0.0720	0.0324	0.0173
8.5	1.07	0.963	0.826	0.748	0.651	0.621	0.512	0.466	0.321	0.214	0.112	0.0646	0.0295	0.0156
9.5	0.952	0.788	0.741	0.660	0.595	0.539	0.450	0.415	0.285	0.188	0.0950	0.058	0.0257	0.0142
11.0	0.859	0.698	0.640	0.594	0.551	0.472	0.416	0.359	0.253	0.169	0.0890	0.0523	0.0238	0.0128
13.0	0.699	0.568	0.531	0.492	0.464	0.395	0.332	0.298	0.209	0.141	0.0738	0.0436	0.0199	0.0109
15.0	0.619	0.515	0.460	0.447	0.374	0.349	0.294	0.275	0.183	0.124	0.0656	0.0385	0.0177	0.00975
17.0	0.527	0.449	0.412	0.391	0.331	0.303	0.258	0.235	0.162	0.109	0.0566	0.0339	0.0155	0.00852
19.0	0.468	0.391	0.359	0.336	0.293	0.270	0.221	0.212	0.144	0.0972	0.0552	0.0302	0.0141	0.00773
22.5	0.390	0.301	0.310	0.279	0.240	0.227	0.194	0.175	0.120	0.0826	0.0466	0.0258	0.0120	0.00654
27.5	0.317	0.270	0.240	0.206	0.196	0.159	0.153	0.143	0.0963	0.0655	0.0371	0.0209	0.00970	0.00507
32.5	0.249	0.200	0.200	0.169	0.165	0.137	0.124	0.106	0.0790	0.0537	0.0291	0.0173	0.00814	0.00444
37.5	0.203	0.162	0.167	0.151	0.136	0.115	0.102	0.0991	0.0655	0.0446	0.0265	0.0146	0.00683	0.00390
42.5	0.185	0.159	0.149	0.120	0.121	0.0989	0.0947	0.0775	0.0596	0.0411	0.0234	0.0134	0.00603	0.00332
45.0	0.171	0.131	0.142	0.109	0.116	0.0902	0.0890	0.0798	0.0560	0.0385	0.0230	0.0130	0.00640	0.00315

TABLE 5

DOSE RATE DATA IN 5-FT CYLINDER
(X_e = 55.9 psf) D_{exp} (mr/hr)/(curie/ft)

ρ(ft) \ h(in.)	1.0	2.0	2.75	3.0	4.25	4.5	5.75	6.0	8.75	11.75	17.75	23.75	35.75	47.75
1.00	7.05	5.6	5.1	4.59	3.9	3.55	2.9	2.65	1.75	0.92	0.41	0.216	0.0920	0.0510
1.75	4.58	3.750	3.310	3.219	2.505	2.522	1.860	1.892	1.132	0.632	0.272	0.144	0.0632	0.0330
2.25			2.571		1.903		1.428		0.830	0.502	0.223	0.123	0.0517	0.0252
2.75	2.832	2.391	2.13	2.045	1.60	1.573	1.17	1.196	0.703	0.421	0.197	0.109	0.0442	0.0225
3.25			1.80		1.328		1.014		0.601	0.374	0.173	0.0944	0.0399	0.0206
3.75	2.088	1.688	1.543	1.451	1.159	1.155	0.886	0.888	0.538	0.333	0.154	0.0872	0.0373	0.0189
4.25			1.355		1.001		0.786		0.478	0.299	0.145	0.0786	0.0336	0.0176
4.75	1.669	1.350	1.201	1.163	0.898	0.919	0.697	0.694	0.421	0.262	0.126	0.0704	0.0308	0.0162
5.25			1.094		0.813		0.635		0.387	0.239	0.116	0.0666	0.0292	0.0153
5.75	1.317	1.103	0.998	0.957	0.731	0.766	0.575	0.586	0.355	0.224	0.108	0.0621	0.0270	0.0145
6.5			0.876		0.663		0.505		0.313	0.197	0.0962	0.0556	0.0246	0.0131
7.5	1.016	0.846	0.765	0.734	0.571	0.587	0.440	0.451	0.279	0.175	0.0854	0.0497	0.0222	0.0117
8.5			0.683		0.51		0.392		0.242	0.155	0.0760	0.0445	0.0198	0.0108
9.5			0.61		0.47		0.35		0.22	0.14	0.0675	0.040	0.0180	0.0095
11.0	0.708	0.588	0.540	0.512	0.427	0.403	0.306	0.327	0.190	0.123	0.0606	0.0359	0.0161	0.00878
13.0			0.439		0.324		0.251		0.160	0.101	0.0504	0.030	0.0135	0.00741
15.0	0.518	0.440	0.386	0.372	0.286	0.303	0.222	0.245	0.138	0.0898	0.0451	0.0267	0.0120	0.00671
17.0			0.346		0.269		0.214		0.122	0.0784	0.0395	0.0236	0.0106	0.00594
19.0	0.409	0.335	0.313	0.291	0.244	0.235	0.173	0.180	0.108	0.0702	0.0350	0.0211	0.00973	0.00529
22.5			0.272		0.188		0.145		0.0896	0.0590	0.0297	0.0179	0.00819	0.00455
27.5	0.273	0.228	0.196	0.201	0.149	0.157	0.116	0.125	0.0726	0.0473	0.0242	0.0144	0.00650	0.00363
32.5			0.162		0.122		0.0995		0.0602	0.0395	0.0201	0.0119	0.00556	0.00309
37.5	0.183	0.154	0.134	0.136	0.108	0.103	0.0791	0.0976	0.0509	0.0338	0.0170	0.0103	0.00484	0.00264
42.5			0.115		0.0903		0.0708		0.0447	0.0299	0.0149	0.00901	0.00437	0.00217
45.0	0.145	0.124	0.11	0.112	0.0807	0.0841	0.069	0.072	0.043	0.0295	0.0145	0.00870	0.00430	0.00210

TABLE 6

DOSE RATE DATA IN 5-FT CYLINDER
($\bar{X}_e$ = 74.5 psf) D_{exp} (mr/hr)/(curie/ft)

h(in.) / ρ(ft)	1.0	2.0	2.75	3.0	4.25	4.5	5.75	6.0	8.75	11.75	17.75	23.75	35.75	47.75
1.00	4.42	4.02	3.60	3.60	2.6	2.55	1.8	1.97	0.97	0.57	0.235	0.122	0.0463	0.0240
1.75	3.377	2.926	2.41	2.373	1.725	1.780	1.361	1.391	0.712	0.421	0.1770	0.0933	0.0387	0.0213
2.25			1.95		1.506		1.152		0.584	0.345	0.1490	0.0801	0.0343	0.0171
2.75	2.141	1.790	1.73	1.518	1.163	1.119	0.872	0.959	0.483	0.293	0.1286	0.0711	0.0315	0.0155
3.25			1.37		1.011		0.756		0.431	0.256	0.1206	0.0640	0.0261	0.0142
3.75	1.630	1.383	1.17	1.179	0.884	0.873	0.664	0.699	0.373	0.225	0.1027	0.0575	0.0239	0.0131
4.25			1.04		0.770		0.573		0.336	0.200	0.0927	0.0525	0.0220	0.0122
4.75	1.309	1.087	0.904	0.922	0.673	0.700	0.514	0.553	0.293	0.1817	0.0857	0.0486	0.0205	0.0115
5.25			0.835		0.620		0.468		0.267	0.1655	0.0775	0.0445	0.0196	0.0108
5.75	1.039	0.874	0.751	0.739	0.557	0.562	0.423	0.431	0.252	0.1527	0.0722	0.0414	0.0178	0.0101
6.5			0.659		0.499		0.380		0.229	0.1355	0.0643	0.0371	0.0160	0.00917
7.5	0.773	0.648	0.581	0.547	0.441	0.422	0.327	0.326	0.1908	0.1198	0.0573	0.0332	0.0145	0.00829
8.5			0.517		0.391		0.295		0.1705	0.1069	0.0512	0.0299	0.0130	0.00757
9.5			0.458		0.342		0.262		0.154	0.0978	0.0470	0.0270	0.0119	0.00700
11.0	0.531	0.440	0.407	0.378	0.292	0.287	0.225	0.229	0.1343	0.0846	0.0411	0.0240	0.0106	0.00621
13.0			0.332		0.240		0.188		0.1105	0.0704	0.0341	0.0201	0.00887	0.00525
15.0	0.394	0.331	0.285	0.281	0.211	0.215	0.165	0.172	0.0987	0.0623	0.0304	0.0180	0.00786	0.00458
17.0			0.248		0.1935		0.1433		0.0856	0.0543	0.0265	0.0158	0.00687	0.00414
19.0	0.277	0.230	0.221	0.196	0.1634	0.154	0.1282	0.119	0.0760	0.0487	0.0238	0.0138	0.00637	0.00371
22.5			0.185		0.1371		0.1073		0.0644	0.0410	0.0200	0.0118	0.00540	0.00319
27.5	0.188	0.154	0.146	0.130	0.1086	0.0988	0.0853	0.0865	0.0510	0.0327	0.0162	0.00972	0.00441	0.00263
32.5			0.1205		0.0898		0.0705		0.0421	0.0274	0.0135	0.00809	0.00372	0.00230
37.5	0.133	0.116	0.1002	0.0956	0.0808	0.0749	0.0598	0.0624	0.0358	0.0231	0.0117	0.00680	0.00307	0.00201
42.5	0.112	0.096	0.0901	0.084	0.0672	0.065	0.0525	0.057	0.0322	0.0206	0.0103	0.00572	0.00264	0.00172
45.0	0.105	0.092	0.086	0.079	0.064	0.060	0.0498	0.052	0.0307	0.0202	0.0099	0.00532	0.00250	0.00162

TABLE 7

DOSE RATE DATA IN 6 FT x 12 FT RECTANGULAR WALL

(X_e = 37.2 psf) D_{exp} (mr/hr)/(curie/ft)

ρ \ φ	0°	20°	40°	55°	70°	80°
			h = 1 in.			
1.00	0.28	0.246	0.228	0.195	0.0720	0.0375
1.75	0.211	0.204	0.164	0.150	0.0546	0.0305
3.75	0.118	0.119	0.0813	0.0677	0.0241	0.0121
7.5	0.0634	0.0602	0.0402	0.0319	0.0102	0.00314
22.5	0.0195	0.0144	0.00876	0.00860	0.00337	0.00137
42.5	0.0099	0.00887	0.00477	0.00436	0.00199	0.00107
45.	0.0095	0.0085	0.00460	0.00420	0.00194	0.00104
			h = 2 in.			
1.00	0.175	0.169	0.150	0.151	0.0650	0.0130
1.75	0.134	0.129	0.111	0.112	0.0451	0.0130
3.75	0.0768	0.0817	0.0578	0.0514	0.0197	0.0113
7.5	0.0410	0.0412	0.0289	0.0235	0.00809	0.00240
22.5	0.0122	0.0110	0.00649	0.00633	0.00262	0.00100
42.5	0.0070	0.00629	0.00347	0.00336	0.00173	0.000867
45.	0.0068	0.00610	0.00339	0.00332	0.00166	0.00084
			h = 3 in.			
1.00	0.1150	0.105	0.101	0.104	0.0540	0.0120
1.75	0.0856	0.0861	0.0818	0.0834	0.0378	0.0120
3.75	0.0528	0.0537	0.0403	0.0387	0.0169	0.0113
7.5	0.0281	0.0290	0.0209	0.0176	0.00656	0.00199
22.5	0.0089	0.00759	0.00409	0.00531	0.00202	0.000885
42.5	0.0044	0.00458	0.00260	0.00198	0.00120	0.000734
45.	0.00425	0.00450	0.00252	0.00182	0.00116	0.000722
			h = 4a in.			
1.00	0.0850	0.0760	0.0750	0.0800	0.0360	0.0120
1.75	0.0643	0.0603	0.0567	0.0593	0.0291	0.0120
3.75	0.0360	0.0401	0.0301	0.0296	0.0137	0.0109
7.5	0.0201	0.0212	0.0151	0.0138	0.00530	0.00188
22.5	0.0072	0.00591	0.00395	0.00405	0.00169	0.000695
42.5	0.0035	0.00343	0.00217	0.00218	0.00106	0.000560
45.	0.0034	0.00332	0.00208	0.00206	0.00104	0.000558

TABLE 7 (Cont'd.)

DOSE RATE DATA IN 6 FT x 12 FT RECTANGULAR WALL

(X_e = 37.2 psf) D_{exp} (mr/hr)/(curie/ft)

ρ \ θ	0°	20°	40°	55°	70°	80°
			h = 48 in.			
1.00	0.0900	0.0960	0.0690	0.0900	0.0595	0.0125
1.75	0.0734	0.0752	0.0651	0.0633	0.0351	0.0125
3.75	0.0381	0.0388	0.0296	0.0301	0.0139	0.0114
7.5	0.0202	0.0206	0.0151	0.0138	0.00548	0.00195
22.5	0.00650	0.00577	0.00444	0.00400	0.00165	0.00075
42.5	0.00365	0.00363	0.00230	0.00220	0.00096	0.00057
45.	0.00340	0.00350	0.00221	0.00212	0.00092	0.00056
			h = 6 in.			
1.00	0.0450	0.0500	0.0390	0.0460	0.0250	0.00900
1.75	0.0360	0.0374	0.0301	0.0337	0.0201	0.00900
3.75	0.0212	0.0215	0.0177	0.0156	0.0101	0.00959
7.5	0.0177	0.0120	0.00914	0.00883	0.00356	0.00122
22.5	0.00396	0.00382	0.00296	0.00263	0.00110	0.000504
42.5	0.00226	0.00224	0.00150	0.00150	0.00064	0.000396
45.	0.00218	0.00218	0.00145	0.00145	0.00061	0.000389
			h = 12 in.			
1.00	0.0140	0.0130	0.0117	0.0145	0.0120	0.0105
1.75	0.01123	0.0113	0.00965	0.0116	0.00936	0.0100
3.75	0.0076	0.00784	0.00648	0.00721	0.00524	0.00601
7.5	0.00476	0.00497	0.00376	0.00370	0.00167	0.000570
22.5	0.00179	0.00162	0.000988	0.000922	0.000462	0.000182
42.5	0.00105	0.00106	0.000759	0.000692	0.000292	0.000163
45.	0.00103	0.00103	0.000750	0.000678	0.000285	0.000160
			h = 24 in.			
1.00	0.00430	0.00440	0.00340	0.00355	0.00358	0.00338
1.75	0.00397	0.00399	0.00314	0.00340	0.0037	0.00320
3.75	0.00307	0.00316	0.00265	0.00307	0.00215	0.00218
7.5	0.00201	0.00204	0.00156	0.00157	0.00069	0.00025
22.5	0.00082	0.00064	0.00061	0.00053	0.00021	0.00010
42.5	0.00050	0.00051	0.00035	0.000315	0.00013	0.000085
45.	0.00049	0.000499	0.00034	0.000309	0.000125	0.000079
			h = 36 in.			
1.00	0.00248	0.00240	0.00158	0.00155	0.00125	0.00195
1.75	0.00211	0.00214	0.00135	0.00149	0.00126	0.00200
3.75	0.00145	0.00150	0.00126	0.00142	0.00139	0.00209
7.5	0.00110	0.00110	0.000830	0.000912	0.000335	0.000123
22.5	0.000465	0.000485	0.000336	0.000282	0.000104	0.0000517
42.5	0.000272	0.000283	0.000193	0.000157	0.0000552	0.0000411
45.	0.000265	0.000280	0.000186	0.000156	0.0000540	0.0000402

TABLE 8

SOLID ANGLE FRACTIONS, ω, AND DETECTOR DEPTHS, h
5 FT CYLINDER AND 6 FT x 12 FT STRUCTURE

h(in.)	Cylinder		Rectangular Structure	
	ω_u	$\omega_{u'}$	ω_u	$\omega_{u'}$
1.00	0.0188	0.917	0.01426	0.808
2.00	0.01821	0.836	0.01388	0.670
2.75	0.01777	0.776		
3.00	0.01767	0.757	0.01356	0.556
4.00			0.01330	0.465
4.25	0.01704	0.666		
4.50	0.01686	0.649		
5.75	0.01633	0.568		
6.00	0.01612	0.553	0.01250	0.340
8.75	0.01497	0.410		
11.75	0.01367	0.286		
12.00			0.01120	0.168
17.75	0.01165	0.171		
23.75	0.01007	0.107		
24.00			0.00862	0.0710
35.75	0.00767	0.052		
36.00			0.00714	0.0385
47.75	0.00610	0.030		

CHAPTER 4

ANALYSIS OF EXPERIMENTAL DATA

INTRODUCTION

The calculational technique based on Spencer's data has proved very useful in evaluating and predicting protection factors of various shelters within the rather wide experimental limits and generally under conditions requiring uncertain extension of the theory. It is therefore desirable to have an unambiguous test of the basic data and assumptions that have gone into the curves of the Engineering Manual.

It will first be necessary to outline the methods of the Manual,[2] and their derivation from Spencer's work, and then to demonstrate how the data that have been collected can be compared with this information. The method of calculating the infinite field dose rate from the experimental data and from the theoretical curves is described. The experimental formulas are given and applied to the data.

DETERMINATION OF DOSE RATE AS A FUNCTION OF SOLID ANGLE

The radiation reaching a detector located in a structure can be divided into three components: direct, air-scattered, and wall-scattered. The direct radiation is the straight-line component from source to detector; the component of air-scattered radiation that has been scattered through large angles is only slightly penetrating and of little consequence in a structure with thick walls and limited open ceiling; the small-angle component, introduced into calculations by the buildup factor, is near the primary in energy and penetration.

The wall-scattered radiation has been deflected, by one or more Compton scatterings, to the detector position and can usefully be considered as originating at the walls. Such an approach is valuable because the dose received at a detector can then be considered proportional to the solid angle of the walls viewed by the detector if the walls have a uniform distribution of radiation. Such an assumption is justified by assuming that the differences in distribution of impinging radiation, above and below the detector line, will be masked by multiple scattering in the wall; therefore, equal solid angles subtended above and below the detector line will yield equal detector responses. The Engineering Manual curves are based on this assumption, which

would be expected to introduce the greatest discrepancy between experiment and theory.

If this assumption is accepted, the dose rate at the detector in a given structure will be a function only of the solid angle subtended by the upper and lower limits of the structure. Then a scattering function $G_s(\omega)$ can be postulated such that the dose rate $D^{\infty} = \alpha(X_e)\left[G_s(\omega_u) + G_s(\omega_{u'})\right]$, where α is a function of the mass thickness and shape of the structure.

Eisenhauer has argued[3] that wall-scattered radiation is close enough to air-scattered radiation in angular distribution to be approximated reasonably well by the already calculated distribution function for air-scattered radiation. Then the wall-scattering function $G_s(\omega)$ is defined as

$$G_s(\omega) = \int_{-(1-\omega)}^{0} \ell(3', \cos\Theta)\, d(\cos\Theta) \qquad (1)$$

$\ell(X, \cos\Theta)$ is plotted on p. 84 of Spencer's monograph.[1] More directly, the curve for $G_s(\omega)$ found in the Engineering Manual is derived from that for $S_a(3', \omega)$ in the Monograph by the relation

$$G_s(\omega) = 0.5\left[1 - S_s(3', \omega)\right]. \qquad (2)$$

The structural constant α has been broken down into $B_w(X_e)S_w(X_e)E$. A barrier shielding factor for the attenuation of radiation by the wall is B_w. The curve in the Engineering Manual is the same as that for W(X,d) in the Monograph multiplied by 2. A weighting factor S_w is described on p. 32 of Eisenhauer's explanatory treatise and represents the fraction of radiation scattered by the wall. Chart 7 of the Engineering Manual plots this weighting factor.

The shape factor E is described by Eisenhauer on p. 31 and is plotted in Chart 8 of the Manual. This factor varies from 1 for a structure with infinitely long walls to $\sqrt{2}$ for a square structure. The variation can be interpreted as the additional

field that would be viewed by a detector in a less eccentric structure through the two walls (in a rectangle) that would be removed to infinity in the structure with walls of infinite length.

Thus a complete system of evaluation has been worked out based on the calculated distribution of radiation intensities scattered into a particular solid angle by a scattering interface. This is expressed in the curve for $G_s(\omega)$ or $S_a(3', \omega)$ modified by expressions for wall thickness and structure shape.

COMPARISON OF THEORY WITH EXPERIMENT

If these theoretical calculations have basis in fact, experimental knowledge of the variation of dose rate with solid angle should allow the comparison of those values with the infinite field dose rate computed from the curve of $S_a(3', \omega)$. The simplest method of comparison is to insert the calculated values of ω_u and $\omega_{u'}$ into the Engineering Manual curve and to compare the result with the measured value. This gives an estimate of the reliability of the composite expression

$$D^{\infty} = 0.5\, S_w B_w E \left[S_a(\omega_{u'}) - S_a(\omega_u) \right].$$

Direct testing of the theoretical values of $S_a(\omega)$ requires additional assumptions to derive an experimental curve. A discussion of this direct testing can be found in Chapter 6 of this report.

CALCULATION OF INFINITE DOSE RATE

The ideal situation involves infinite structures surrounded by infinite fields of radiation. The field is in actuality limited by time and the bounds of the testing area. Experimental determination of a rapid convergence toward complete response with structure height, expressible by the approximation of the solid angle subtended by the upper limit to zero, indicated that the practical limits of the structure were adequate.

The problem of a finite cylinder can be accounted for in the comparison with $S_a(3', \omega)$, but the contribution of the field beyond 45 ft amounted to a third or more of the total dose rate and required careful estimation based on theory and on data

from the field within 45 ft. As has been discussed in Chapter 2 of this report, a plane circular field about a cylinder can be represented by a succession of radial points. The measured dose rate from each point is multiplied by $2\pi r\Delta r$ to give the dose rate from an annular ring. The total dose rate from a plane source is then found by summing these rings. The only inaccuracy lies in the finite size of Δr. An additional inaccuracy is introduced in the experiment with the rectangular wall when the field is simulated by a succession of radial lines at different angles to the wall and is separated by a finite $\Delta\phi$.

As was shown, the contribution from each annular ring is equivalent to the derivative of the total dose with distance dD/dr at that radial distance. Then a point source qS_o at a distance r from a detector on the axis of a cylinder will represent an area source to give a gradient

$$\frac{dD}{dr} = \frac{2\pi qS_o e^{-\mu r} B(\mu r)}{r}\left[g_s(\omega_u) - g_s(\omega_{u'})\right] \tag{3}$$

where $g_s(\omega)$ is a general scattering function, assumed independent of r for large r, and $B(\mu r)$ is a buildup factor generally dependent on r.

If a functional form can be found for $B(\mu r)$, Eq. (3) can in theory be integrated over a range of r through which r is large enough to have given Δg_s its independence of r. Then the contribution from this area to the dose rate will be

$$D(r_1, r_2) = \int_{r_1}^{r_2} \frac{2\pi qS_o B(\mu r)}{r} e^{-\mu r} dr \cdot \Delta g_s. \tag{4}$$

If it is found that Δg_s reaches its asymptotic value at a distance equal to, or less than, the greatest experimental distance r_o, then r_1 can be set equal to r_o, $r_2 = \infty$ and

$$D^{\infty} = D(r = r_o) + 2\pi qS_o \int_{r_o}^{\infty} \frac{e^{-\mu r}}{r} B(\mu r) dr \cdot \Delta g_s \tag{5}$$

where $D(r = r_o)$ is the dose rate from a field out to r_o. Thus the infinite field dose rate can be calculated if $B(\mu r)$ is known analytically and is reasonably simple and if the asymptotic value of Δg_s can be found.

In traversing a medium, in this case air, a beam of radiation is attenuated by two principal mechanisms at this energy: (1) photoelectric absorption, in which the photon is permanently removed from the beam, and (2) Compton scattering, which can occur a number of times and which may eventually scatter the photon back into the solid angle viewed by the detector. In a narrow-beam attenuation experiment, the total absorption coefficient for a particular material and photon energy is measured, but this coefficient in fact is made up of an energy absorption and a scattering coefficient. The energy absorption process follows a straight exponential decrease for each element of the radiation field, but this must be modified by a factor representing the radiation scattered back into the beam, the buildup factor. Thus,

$$D = D_o e^{-\mu_T r} \frac{B(\mu r)}{r^2}.$$

Experiments on the air-scatter of Co-60 radiation[5] have led to a least-squares, best-fit linear approximation of the buildup factor $B(\mu r) = 1 + 0.7(\mu r)^{0.72}$. This was chosen as one expression for $B(\mu r)$ with $\mu = \mu_T$. As another extreme, $B(\mu r) = 1$ was chosen, assuming that no scattered radiation rejoined the beam; a third choice was $B(\mu r) = 1$, $\mu = \mu_A$, assuming no scattering took place at all. It was hoped that the experimental values of D^∞ found by each of these approaches would be close together and would bracket the correct expression among them. The three approaches then were:

1. $B(\mu r) = 1 + 0.7(\mu r)^{0.72}$ $\mu = \mu_T$ = total (narrow beam) absorption coefficient
2. $B(\mu r) = 1$ $\mu = \mu_T$
3. $B(\mu r) = 1$ $\mu = \mu_A$ = energy absorption coefficient.

As a derivation of asymptotic scattering function $g_s(\omega)$, Eq. (5) can thus be integrated and used if Δg_s can be calculated from the data available and is found essentially independent of r at the furthest measurement made.

The dose rate at a detector on the cylinder axis from wall-scattered radiation may be written:

$$\frac{dD}{dr} = 2\pi r q S_o \int_{\omega_{u'}}^{\omega_u} d\omega \int_0^{2\pi} \frac{e^{-\mu\rho} B(\mu\rho)}{\rho^2} \alpha(X_e, \Theta_o, \Theta, \phi) \frac{\cos \Theta_o}{\cos \Theta} a \, d\phi \qquad (6)$$

where

r = radial distance from axis to source

S_o = RHF = 14.0 r/hr/curie at 1 ft from Co-60

q = source density, curies/ft^2

$2\pi q S_o$ = 87.92 for q = 1 curie/ft^2

μ = absorption coefficient, ft^{-1}

ρ = slant distance from the source to the scattering area, ft

$$= \left[r^2 + h^2 + \frac{a^2}{\sin^2 \Theta} - 2 \frac{a}{\sin \Theta} (h \cos \Theta + r \sin \Theta \cos \phi \right]^{1/2}$$

e = cylinder height

h = detector depth

a = cylinder radius

$\alpha(X_e, \Theta_o, \Theta, \phi)$ = dose scattering function, steradian^{-1}

$$\omega_u = 1 - \frac{h + e}{\sqrt{(h + e)^2 + a^2}}$$

$$\omega_{u'} = 1 - \frac{h}{\sqrt{h^2 + a^2}}.$$

As r becomes much larger than a and $\rho \approx r$, independent of Θ and ϕ, then Eq. (6) becomes

$$\frac{dD}{dr} = \frac{2\pi r q S_o e^{-\mu r} B(\mu r)}{r^2} \int_{\omega_{u'}}^{\omega_u} \frac{a}{\cos\Theta} \int_0^{2\pi} \alpha(X_e, \Theta_o, \Theta, \phi) \cos\Theta \, d\omega \, d\phi. \qquad (7)$$

The integral in Eq. (7) is independent of r. If a function $g_s(X_e, \omega)$ is defined such that

$$g_s(X_e, \omega) = \int_0^{\omega} \frac{a}{\cos\Theta} \int_0^{2\pi} \alpha(X_e, \Theta_o, \Theta, \phi) \cos\Theta_o \, d\omega \, d\phi, \qquad (8)$$

then

$$\frac{dD}{dr} = \frac{2\pi q S_o e^{-\mu r} B(\mu r)}{r} \left[g_s(X_e, \omega_u) - g_s(X_e, \omega_{u'}) \right] \qquad (9)$$

where $g_s(X_e, \omega)$ represents the scattering properties of the part of the cylinder above ω, in a field of radiation beginning a distance r_o from the cylinder axis.

The quantity actually measured in this experiment is dD/dr. If the assumptions made above are correct, the experimental data for a given detector position multiplied by $r/\left[2\pi q S_o e^{-\mu r} B(\mu r)\right]$ should asymptotically approach a constant value for radii large with respect to the cylinder radius. This value is Δg_s, which can then be used in Eq. (5) to find the infinite field dose. The result of this computation for the 1/2-in. thick cylinder is shown in Figure 6. The curves are found to approach an asymptotic value as r increases.

Table 9 lists Δg_s and D^{∞} for two cylinder wall thicknesses, showing fairly close agreement among the three approaches and the expected bracketing of the dose rate incorporating buildup by the two extreme cases.

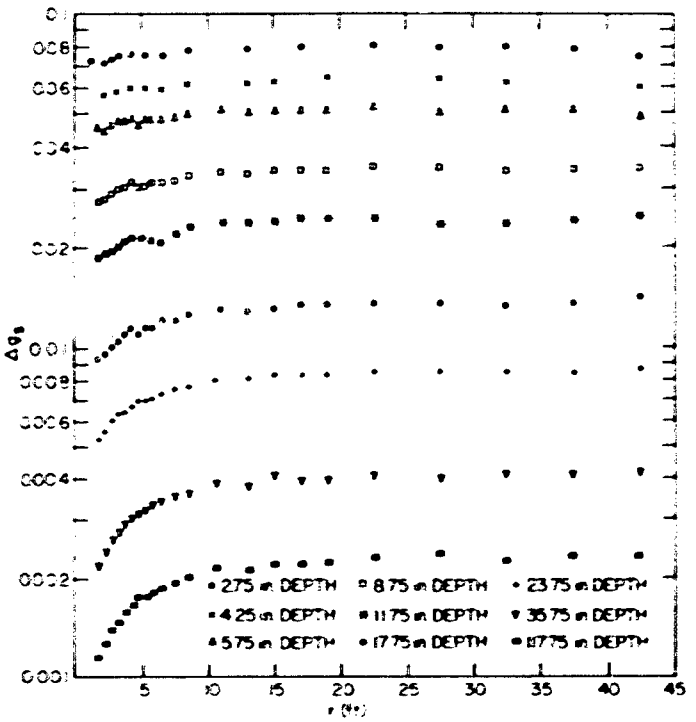

Figure 6. $\frac{D_{exp} \cdot r}{2\pi q S_o e^{-\mu r} B(\mu r)}$ vs r, X_e = 18.6 psf, $B(\mu r) = 1$, $\mu = \mu_T$

TABLE 9

ASYMPTOTIC SCATTERING FUNCTION $\Delta g_s(X_e, \omega)$ AND INFINITE-FIELD DOSE RATE FOR CYLINDER WALL THICKNESSES OF 18.6 AND 74.5 PSF USING DIFFERENT FUNCTIONS FOR $B(\mu r)$ AT DETECTOR DEPTH OF 11.75 IN.

Scattering Function and Dose Rate	X_e(psf)	$B(\mu r) = 1 + 0.7(\mu r)^{0.72}$ $\mu = \mu_T$	$B(\mu r) = 1$ $\mu = \mu_T$	$B(\mu r) = 1$ $\mu = \mu_A$
Δg_s	18.6	0.0214	0.0239	0.0230
D^∞		11.17	10.26	11.54
Δg_s	74.5	0.00959	0.0109	0.0105
D^∞		5.13	4.75	5.33

CALCULATION OF D^{∞} BY THE ENGINEERING MANUAL METHOD

The basic equation accounting for wall-scattered radiation is

$$\frac{D^{\infty}}{D_o} = B_w S_w E \left[G_s(\omega_u) - G_s(\omega_{u'}) \right]$$

or

$$\frac{D^{\infty}}{D_o} = 0.5\, B_w S_w E \left[S_a(\omega_{u'}) - S_a(\omega_u) \right].$$

However, the experimental measurements include air-scattered radiation expressed as the buildup factor in the derivation of the far-field dose rate that must be taken into account as

$$\frac{D^{\infty}_{ss}}{D_o} = B_w(1 - S_w) \left[G_a(\omega_u) - G_a(\omega_{u'}) \right] = \frac{0.088\, B_w}{D_o} (1 - S_w) \left[S_a(\omega_{u'}) - S_a(\omega_u) \right], \tag{10}$$

since there is no ceiling scatter contribution. The complete equation then becomes

$$\begin{aligned} \frac{D^{\infty}}{D_o} &= 0.5 B_w S_w E \left[S_a(\omega_{u'}) - S_a(\omega_u) \right] \\ &\quad + 0.088 B_w(1 - S_w) \left[S_a(\omega_{u'}) - S_a(\omega_u) \right] + 0.088\, \omega_u. \end{aligned} \tag{11}$$

The last term represents the radiation scattered directly through the top opening of the cylinder. Since it is very small, less than 3% of the total even at the highest position in the thickest cylinder, it can be neglected.

Equation (11) implies quite a difference in approach between the experimental and theoretical calculations for air-scatter effects. Experimentally, air-scattered radiation was handled as a multiplicative factor modifying the radiation flux at the scattering wall, ignoring air-scattered radiation striking the detector directly. The

Engineering Manual considers this radiation as an additive term dealing with direct air-scattered radiation only, attenuated but not scattered by the intervening wall. Since it would be difficult to separate experimentally the effects of air-scattered and direct wall-scattered radiation, the Engineering Manual approach doesn't exactly mirror the physical situation. Theoretical calculations indicate that skyshine is about 10% of the total for the thinnest (1/2 in.) walls; experiments indicate 6%. There is closer agreement for thicker structures, pointing to a maximum error of 4% through accounting for skyshine.

Equation (11) can be reduced to

$$\frac{D^{\infty}}{D_o} = B_w \left[S_a(\omega_{u'}) - S_a(\omega_u) \right] \left[0.5 S_w E + 0.088(1 - S_w) \right] \qquad (12)$$

for final calculations.

PRESENTATION OF EXPERIMENTAL FORMULAS

Dose rate was measured out to 42.5 ft, and an extrapolated value at 45 ft was used. As shown in Figure 6, $\Delta g_s(X_e, \omega)$ appears to have reached a constant value at this distance; also, the greater part of D^{∞} (~ 2/3 of it) is contributed by the radiation within 45 ft. This is particularly important as the greatest source of error seems to be in the determination of Δg_s.

Another major problem, that of buildup factor, was handled by attempting to bracket it by three sets of assumptions:

1. $\mu = \mu_{total} \rightarrow \lambda = 445$ ft $B(\mu r) = 1 + 0.7(\mu r)^{0.72}$
2. $\mu = \mu_{total}$ $B(\mu r) = 1$
3. $\mu = \mu_{abs} \rightarrow \lambda = 947.2$ ft $B(\mu r) = 1$

where λ is the mean free path in air.[6]

This leads to three separate solutions of the integral in Eq. (3):

1. $$2\pi qS_o \int_{45}^{\infty} \frac{e^{-r/445}}{r} \left[1 + 0.7\left(\frac{r}{445}\right)^{0.72}\right] dr$$

$$= 2\pi qS_o \left[E_1\left(\frac{45}{445}\right) + 0.7 \int_{45}^{\infty} \left(\frac{r}{445}\right)^{-0.28} e^{-\frac{r}{445}} dr\right] = 220.7$$

2. $$2\pi qS_o \int_{45}^{\infty} \frac{e^{-r/445}}{r} \cdot 1\, dr = 2\pi qS_o\left(\frac{45}{445}\right) = 159.4 \qquad (13)$$

$$2\pi qS_o \int_{45}^{\infty} \frac{e^{-r/947.2}}{r} \cdot 1\, dr = 2\pi qS_o\left(\frac{45}{947.2}\right) = 221.3,$$

and three expressions for D^{∞}

1. $$D_1^{\infty} = D(\rho = 45) + 220.7\left[g_s^1(\omega_u) - g_s^1(\omega_{u'})\right]$$

2. $$D_2^{\infty} = D(\rho = 45) + 159.4\left[g_s^2(\omega_u) - g_s^2(\omega_{u'})\right] \qquad (14)$$

3. $$D_3^{\infty} = D(\rho = 45) + 221.3\left[g_s^3(\omega_u) - g_s^3(\omega_{u'})\right].$$

Finally, Eq. (6) must be put into three forms:

1. $$\left[g_s^1(\omega_u) - g_s^1(\omega_{u'})\right] = \frac{r}{87.92\, e^{-r/445}\left[1 + 0.7/445(\mu r)^{0.72}\right]} \frac{dD}{dr}$$

2. $$\left[g_s^2(\omega_u) - g_s^2(\omega_{u'})\right] = \frac{r}{87.92\, e^{-r/445}} \frac{dD}{dr} \qquad (15)$$

3. $$\left[g_s^3(\omega_u) - g_s^3(\omega_{u'})\right] = \frac{r}{87.92\, e^{-r/947.2}} \frac{dD}{dr}$$

to find the proper value of $g_s(\omega, r \to \infty)$.

The dose rate from the rectangular wall was computed using the first assumption, giving

$$D_1^{\infty} = \sum_{\phi} D(\phi)$$

where

$$D(\phi) = \sum_{r} D(r,\phi) + 35.12\left[g_s(\omega_u,\phi) - g_s(\omega_{u'},\phi)\right]\Delta\phi.$$

Since the response of the wall would be symmetric about the perpendicular to the wall, measurements were made only in one quadrant and the resulting dose rate multiplied by four to simulate a structure with two infinitely long, parallel walls.

The solid angle subtended by this structure was computed using the formula presented on p. 68 of Spencer's Monograph for one surface and multiplying this by two. The effect of the smaller size of the detector hole on the solid angle was found by treating the resultant complicated shape as a composite of simpler ones.

EXPERIMENTAL AND CALCULATED VALUES OF D^{∞}

The raw data, $D_{exp}(r)$, is presented in Table 4. In Table 10 D(r) is multiplied by Δr and is summed from 1 ft to 45 ft to give detector response from a plane source in that area; i.e., D(r = 45). In Table 11 $D_{exp} \cdot r/2\pi qS_o e^{-\mu r} B(\mu r)$ is presented for the 1/2 in.-thick cylinder, and is plotted against r in Figure 6. Tables 12 and 13 present the asymptotic values of Δg_s, D(r = 45), and the values of $D^{\infty}(\omega)$ corresponding to the three Eq. (15), for each value of X_e and structure shape. Calculated values of D^{∞}/D_o are presented in Table 14 and are compared with the experimental results in Table 15.

The variation of $D^{\infty}(\omega)$ with ω in the 1 in. cylinder is shown in Figure 7. An extrapolated value of D^{∞} at $\omega = 1$ can be derived from this plot to give an experimental estimate of $B_w\left[0.5S_wE + 0.088(1 - S_w)\right]$; however, a more consistent method appeared to be the approximation of the dose-rate points by an analytic function of ω_1 as described on p. 45. The variation of dose rate with solid angle predicted by the theory is compared with the experimental values in Figure 8.

TABLE 10

D(r=45). SUMMATION OF DOSE RATES FROM ANNULAR RINGS OF RADIATION FROM 1 TO 45 FT; 1/2 IN. CYLINDER

r(ft)	Depth (in.) / Δr	1.0		2.0		2.75		3.0		4.25		4.5		5.75	
		a*	b†	a	b	a	b	a	b	a	b	a	b	a	b
1.00	0.75	6.65	4.987	5.6	4.20	4.394	3.295	4.67	3.502	3.21	2.407	3.62	2.715	2.512	1.884
1.75	0.5	4.55	2.275	3.9	1.95	3.203	1.602	3.23	1.615	2.325	1.162	2.56	1.28	1.972	0.986
2.25	0.5	3.55	1.775	3.05	1.53	2.575	1.287	2.55	1.275	1.99	0.995	2.00	1.00	1.572	0.786
2.75	0.5	3.0	1.5	2.5	1.25	2.175	1.088	2.15	1.075	1.66	0.830	1.67	0.835	1.350	0.675
3.25	0.5	2.6	1.3	2.15	1.07	1.874	0.937	1.79	0.895	1.475	0.737	1.46	0.73	1.172	0.586
3.75	0.5	2.25	1.125	1.9	0.95	1.617	0.808	1.56	0.78	1.305	0.653	1.30	0.65	1.029	0.514
4.25	0.5	1.95	0.975	1.7	0.85	1.437	0.719	1.38	0.69	1.155	0.577	1.14	0.57	0.908	0.454
4.75	0.5	1.75	0.875	1.5	0.75	1.278	0.639	1.27	0.635	1.035	0.518	1.03	0.515	0.816	0.408
5.25	0.5	1.6	0.80	1.35	0.68	1.168	0.584	1.14	0.57	0.937	0.468	0.935	0.467	0.751	0.376
5.75	0.75	1.4	1.05	1.2	0.90	1.049	0.787	1.01	0.757	0.837	0.628	0.802	0.601	0.674	0.505
6.5	1.0	1.25	1.25	1.05	1.05	0.921	0.921	0.942	0.945	0.744	0.744	0.709	0.709	0.595	0.595
7.5	1.0	1.15	1.15	0.95	0.95	0.819	0.819	0.805	0.805	0.660	0.660	0.649	0.649	0.525	0.525
8.5	1.0	1.03	1.03	0.85	0.85	0.746	0.746	0.708	0.708	0.602	0.602	0.575	0.575	0.468	0.468
9.5	1.5	0.915	1.373	0.77	1.155	0.639	0.958	0.639	0.958	0.518	0.777	0.512	0.768	0.417	0.625
11.0	2.0	0.775	1.55	0.665	1.33	0.546	1.092	0.545	1.09	0.431	0.862	0.444	0.888	0.362	0.724
13.0	2.0	0.64	1.28	0.55	1.10	0.475	0.950	0.457	0.914	0.383	0.766	0.371	0.742	0.309	0.618
15.0	2.0	0.565	1.13	0.485	0.97	0.416	0.832	0.408	0.816	0.335	0.670	0.330	0.660	0.264	0.528
17.0	2.0	0.50	1.0	0.43	0.86	0.373	0.746	0.360	0.72	0.298	0.596	0.294	0.588	0.231	0.462
19.0	3.5	0.425	1.487	0.365	1.277	0.325	1.137	0.304	1.064	0.262	0.917	0.247	0.864	0.208	0.728
22.5	5.0	0.345	1.725	0.30	1.50	0.270	1.35	0.249	1.245	0.214	1.07	0.200	1.00	0.171	0.855
27.5	5.0	0.28	1.4	0.245	1.225	0.219	1.095	0.204	1.02	0.177	0.885	0.165	0.825	0.138	0.690
32.5	5.0	0.24	1.2	0.207	1.035	0.184	0.92	0.169	0.845	0.148	0.74	0.142	0.71	0.119	0.595
37.5	5.0	0.21	1.05	0.174	0.870	0.156	0.78	0.145	0.725	0.123	0.615	0.122	0.61	0.100	0.500
42.5	2.5	0.185	0.463	0.155	0.387	0.138	0.345	0.132	0.330	0.111	0.277	0.109	0.272	0.087	0.217
			33.750		28.689		24.437		23.979		19.156		19.273		15.305

*a = $D_1 + D_2/2$; D_1 = dose rate at r; D_2 = dose rate at r + Δr

†b = $D_1 + D_2/2 \cdot \Delta r$

TABLE 10 (Cont'd.)

D(r=45). SUMMATION OF DOSE RATES FROM ANNULAR RINGS OF RADIATION FROM 1 TO 45 FT; 1/2 IN. CYLINDER

r(ft)	Depth (in.) / Δr	6.0		8.75		11.75		17.75		23.75		35.75		47.75	
		a*	b†	a	b	a	b	a	b	a	b	a	b	a	b
1.00	0.75	2.74	2.055	1.625	1.219	1.071	0.803	0.579	0.434	0.303	0.227	0.130	0.0975	0.0673	0.0505
1.75	0.5	1.99	0.995	1.236	0.618	0.832	0.416	0.419	0.209	0.241	0.120	0.1025	0.0512	0.0528	0.0264
2.25	0.5	1.56	0.78	1.007	0.503	0.681	0.340	0.347	0.174	0.204	0.102	0.0886	0.0443	0.0463	0.0231
2.75	0.5	1.29	0.645	0.864	0.432	0.587	0.294	0.300	0.150	0.181	0.091	0.0789	0.0395	0.0417	0.0209
3.25	0.5	1.12	0.56	0.758	0.379	0.522	0.261	0.267	0.133	0.160	0.080	0.0712	0.0356	0.0380	0.0190
3.75	0.5	0.992	0.496	0.675	0.338	0.468	0.234	0.243	0.122	0.143	0.071	0.0653	0.0320	0.0351	0.0175
4.25	0.5	0.894	0.447	0.607	0.301	0.419	0.209	0.217	0.108	0.131	0.066	0.0600	0.0300	0.0327	0.0164
4.75	0.5	0.810	0.405	0.539	0.270	0.376	0.188	0.196	0.098	0.120	0.060	0.0555	0.0278	0.0305	0.0152
5.25	0.5	0.728	0.364	0.494	0.247	0.343	0.172	0.181	0.090	0.111	0.055	0.0521	0.0260	0.0283	0.0142
5.75	0.75	0.649	0.487	0.445	0.334	0.302	0.226	0.167	0.125	0.102	0.0765	0.0480	0.0360	0.0262	0.0196
6.5	1.0	0.580	0.580	0.393	0.393	0.268	0.268	0.149	0.149	0.0919	0.0919	0.0432	0.0432	0.0235	0.0235
7.5	1.0	0.521	0.521	0.352	0.352	0.245	0.245	0.132	0.132	0.0822	0.0822	0.0389	0.0389	0.0213	0.0213
8.5	1.0	0.457	0.457	0.313	0.313	0.222	0.222	0.121	0.121	0.0740	0.0740	0.0354	0.0354	0.0196	0.0196
9.5	1.5	0.416	0.624	0.279	0.418	0.199	0.298	0.101	0.151	0.0667	0.100	0.0319	0.0478	0.0178	0.0267
11.0	2.0	0.363	0.726	0.240	0.480	0.171	0.342	0.0921	0.1842	0.0580	0.1160	0.0275	0.0550	0.0153	0.0306
13.0	2.0	0.296	0.592	0.205	0.410	0.147	0.294	0.0788	0.1576	0.0498	0.0996	0.0237	0.0474	0.0131	0.0262
15.0	2.0	0.265	0.530	0.182	0.364	0.128	0.256	0.0703	0.1406	0.0439	0.0878	0.0210	0.0420	0.0116	0.0232
17.0	2.0	0.233	0.466	0.161	0.322	0.115	0.230	0.0624	0.1248	0.0388	0.0776	0.0187	0.0374	0.01034	0.0207
19.0	3.5	0.195	0.682	0.140	0.490	0.100	0.350	0.0525	0.1907	0.0339	0.1186	0.0164	0.0574	0.00919	0.0322
22.5	5.0	0.160	0.80	0.116	0.580	0.0824	0.412	0.0454	0.227	0.0284	0.142	0.0136	0.0680	0.00776	0.0388
27.5	5.0	0.131	0.655	0.0939	0.469	0.0659	0.329	0.0370	0.185	0.0233	0.116	0.0112	0.0560	0.00638	0.0319
32.5	5.0	0.111	0.555	0.0790	0.395	0.0553	0.277	0.0312	0.156	0.0195	0.098	0.00963	0.0481	0.00538	0.0269
37.5	5.0	0.1018	0.509	0.0691	0.346	0.0492	0.246	0.0276	0.138	0.0171	0.085	0.00835	0.0418	0.00473	0.0236
42.5	2.5	0.087	0.217	0.0625	0.156	0.0458	0.114	0.0256	0.0637	0.0156	0.039	0.00761	0.0190	0.00427	0.0107
			15.148		10.129		7.026		3.764		2.276		1.057		0.5786

*a = $D_1 + D_2/2$; D_1 = dose rate at r; D_2 = dose rate at r + Δr

†b = $D_1 + D_2/2 \cdot \Delta r$

TABLE 11

$$\frac{D_{exp} \cdot r}{2\pi\varphi S_o e^{-\rho r} B(\mu r)} = \text{1/2-in. CYLINDER}$$

in. / ρ	1.0			2.0			2.75			3.0		
	a*	b†	c‡	a	b	c	a	b	c	a	b	c
1.75		0.104	0.1037		0.088	0.0877		0.0718	0.0716		0.0730	0.0728
2.25		0.100	0.1000		0.0874	0.0872		0.0718	0.0723		0.0720	0.0718
2.75		0.101	0.1004		0.085	0.0847		0.0735	0.0731		0.0724	0.0722
3.25		0.104	0.1039		0.0856	0.0853		0.0751	0.0748		0.0718	0.0716
3.75		0.103	0.1028		0.0860	0.0857			0.0741		0.0709	0.0707
4.25		0.102	0.1020		0.0878	0.0804		0.0758	0.0755		0.0712	0.0709
4.75		0.0983	0.0977		0.0874	0.0869			0.0717		0.0715	0.0711
5.25		0.103	0.102		0.0846	0.0840		0.0747	0.0742		0.0737	0.0732
5.75		0.0993	0.0990		0.0861	0.0858			0.0726		0.0708	0.0706
6.5		0.0975	0.0968		0.0825	0.0819		0.0748	0.0742		0.0712	0.0707
7.5		0.104	0.103		0.0868	0.0860			0.0727		0.0741	0.0734
8.5		0.108	0.107		0.0886	0.0878		0.0781	0.0773		0.0745	0.0738
11.0		0.112	0.110		0.0949	0.0937			0.0732		0.0792	0.0782
13.0		0.104	0.102		0.0899	0.0884		0.0784	0.0771		0.0736	0.0724
15.0	0.0934	0.106	0.104	0.0794	0.0900	0.0884	0.0677		0.0754	0.0671	0.0761	0.0747
17.0	0.0940	0.106	0.104	0.0816	0.0924	0.0906	0.0705	0.0799	0.0783	0.0683	0.0773	0.0758
19.0	0.0937	0.106	0.103	0.0797	0.0902	0.0891	0.0696		0.0769	0.0670	0.0758	0.0740
22.5	0.0904	0.102	0.0995	0.0785	0.0888	0.0864	0.0717	0.0810	0.0789	0.0647	0.0732	0.0712
27.5	0.0908	0.103	0.0997	0.0791	0.0899	0.0868	0.0697	0.0792	0.0765	0.0662	0.0752	0.0727
32.5	0.0871	0.0994	0.0958	0.0767	0.0875	0.0843	0.0695	0.0795	0.0764	0.0634	0.0724	0.0697
37.5	0.0929	0.107	0.1022	0.0783	0.0900	0.0862	0.0682	0.0784	0.0751	0.0630	0.0724	0.0693
42.5	0.0874	0.101	0.0960	0.0736	0.0851	0.0808	0.0655	0.0755	0.0719	0.0621	0.0718	0.0682

*$B(\mu r) = 1 + 0.7(\mu r)^{0.72}$ $\mu = \mu_T = 1/445$ ft.

†$B(\mu r) = 1$ $\mu = \mu_T = 1/445$ ft.

‡$B(\mu r) = 1$ $\mu = \mu_A = 1/947.2$ ft.

TABLE 11 (Cont'd.)

$$\frac{D_{exp} \cdot r}{2\pi q S_o e^{-\mu r} B(\mu r)} = \text{1/2-in. CYLINDER}$$

in. / ρ	4.25			4.5			5.75			6.0		
	a*	b†	c‡	a	b	c	a	b	c	a	b	c
1.75			0.0483		0.0588	0.0586		0.0449	0.0447		0.0456	0.0455
2.25		0.0573	0.0572		0.0563	0.0562		0.0437	0.0436		0.0439	0.0439
2.75			0.0549		0.0567	0.0565		0.0454	0.0452		0.0441	0.0439
3.25		0.0584	0.0582		0.0573	0.0571		0.0468	0.0467		0.0443	0.0441
3.75			0.0591		0.0598	0.0595		0.0467	0.0466		0.0451	0.0450
4.25		0.0600	0.0597		0.0590	0.0588		0.0474	0.0472		0.0456	0.0454
4.75			0.0586		0.0584	0.0581		0.0461	0.0458		0.0465	0.0462
5.25		0.0599	0.0595		0.0602	0.0598		0.0476	0.0473		0.0464	0.0461
5.75			0.0582		0.0578	0.0576		0.0473	0.0471		0.0455	0.0454
6.5		0.0595	0.0590		0.0549	0.0545		0.0476	0.0473		0.0458	0.0455
7.5			0.0598		0.0596	0.0591		0.0481	0.0476		0.0476	0.0471
8.5		0.0615	0.0609		0.0601	0.0595		0.0490	0.0485		0.0487	0.0482
11.0			0.0577		0.0633	0.0625		0.0509	0.0503		0.0528	0.0522
13.0		0.0620	0.0610		0.0600	0.0591		0.0498	0.0490		0.0478	0.0471
15.0	0.0559	0.0628	0.0622	0.0542	0.0614	0.0603	0.0452	0.0512	0.0503	0.0433	0.0491	0.0482
17.0	0.0553		0.0614	0.0562	0.0637	0.0624	0.0422	0.0504	0.0469	0.0449	0.0508	0.0498
19.0	0.0568	0.0643	0.0628	0.0546	0.0611	0.0597	0.0448	0.0508	0.0496	0.0423	0.0478	0.0467
22.5	0.0568		0.0623	0.0531	0.0600	0.0584	0.0457	0.0517	0.0503	0.0424	0.0479	0.0466
27.5	0.0558	0.0636	0.0612	0.0521	0.0592	0.0572	0.0436	0.0496	0.0479	0.0419	0.0476	0.0460
32.5	0.0568		0.0624	0.0526	0.0600	0.0578	0.0446	0.0509	0.0490	0.0415	0.0473	0.0456
37.5	0.0535	0.0617	0.0589	0.0537	0.0617	0.0591	0.0440	0.0506	0.0484	0.0419	0.0482	0.0461
42.5	0.0523	0.0606	0.0574	0.0515	0.0596	0.0566	0.0420	0.0486	0.0462	0.0414	0.0478	0.0454

*$B(\mu r) = 1 + 0.7(\mu r)^{0.72}$ $\mu = \mu_T = 1/445$ ft.

†$B(\mu r) = 1$ $\mu = \mu_T = 1/445$ ft.

‡$B(\mu r) = 1$ $\mu = \mu_A = 1/947.2$ ft.

TABLE 11 (Cont'd.)

$$\frac{D_{exp} \cdot r}{2\pi q S_o e^{-\mu r} B(\mu r)} = \text{1/2-in. CYLINDER}$$

in. / ρ	8.75			11.75			17.75		
	a*	b†	c‡	a	b	c	a	b	c
1.75		0.0276	0.0275		0.0185	0.0184		0.00928	0.00925
2.25		0.0281	0.0280		0.0190	0.0190		0.00951	0.00959
2.75		0.0291	0.0289		0.0196	0.0195		0.0101	0.01004
3.25		0.0300	0.0299		0.0206	0.0205		0.0104	0.01039
3.75		0.0304	0.0303		0.0211	0.0210		0.0109	0.01088
4.25		0.0314	0.0312		0.0218	0.0217		0.0113	0.01080
4.75		0.0307	0.0306		0.0215	0.0213		0.0111	0.01108
5.25		0.0310	0.0309		0.0217	0.0216		0.0114	0.01128
5.75		0.0314	0.0313		0.0214	0.0215		0.0115	0.01148
6.5		0.0313	0.0310		0.0209	0.0208		0.0119	0.01184
7.5		0.0322	0.0319		0.0223	0.0221		0.0121	0.01200
8.5		0.0327	0.0324		0.0230	0.0227		0.0123	0.01220
11.0		0.0337	0.0333		0.0238	0.0235		0.0129	0.0128
13.0		0.0330	0.0325		0.0239	0.0235		0.0127	0.0125
15.0	0.0301	0.0341	0.0334	0.0212	0.0240	0.0236	0.0116	0.0131	0.0129
17.0	0.0302	0.0342	0.0335	0.0215	0.0243	0.0238	0.0117	0.0133	0.0130
19.0	0.0303	0.0341	0.0335	0.0215	0.0244	0.0238	0.0117	0.0133	0.0130
22.5	0.0307	0.0347	0.0339	0.0219	0.0248	0.0241	0.0119	0.0135	0.0131
27.5	0.0302	0.0343	0.0331	0.0214	0.0243	0.0234	0.0119	0.0135	0.0117
32.5	0.0295	0.0337	0.0325	0.0205	0.0234	0.0226	0.0116	0.0133	0.0128
37.5	0.0296	0.0340	0.0326	0.0215	0.0240	0.0230	0.0117	0.0134	0.0128
42.5	0.0299	0.0345	0.0328	0.0219	0.0248	0.0236	0.0121	0.0130	0.0133

* $B(\mu r) = 1 + 0.7(\mu r)^{0.72}$ $\mu = \mu_T = 1/445$ ft.

† $B(\mu r) = 1$ $\mu = \mu_T = 1/445$ ft.

‡ $B(\mu r) = 1$ $\mu = \mu_A = 1/947.2$ ft.

TABLE 11 (Cont'd.)

$$\frac{D_{exp} \cdot r}{2\pi q S_o e^{-\mu r} B(\mu r)} = \text{1/2-in. CYLINDER}$$

ρ \ in.	23.75			35.75			47.75		
	a*	b†	c‡	a	b	c	a	b	c
1.75		0.00530	0.00528		0.00222	0.00221		0.00113	0.00113
2.25		0.00558	0.00557		0.00242	0.00241		0.00126	0.00125
2.75		0.00602	0.00599		0.00262	0.00261		0.00138	0.00137
3.25		0.00632	0.00631		0.00277	0.00276		0.00147	0.00147
3.75		0.00641	0.00638		0.00292	0.00291		0.00157	0.00156
4.25		0.00669	0.00665		0.00305	0.00304		0.00165	0.00164
4.75		0.00688	0.00679		0.00313	0.00312		0.00173	0.00172
5.25		0.00695	0.00690		0.00324	0.00322		0.00177	0.00176
5.75		0.00702	0.00706		0.00334	0.00333		0.00181	0.00181
6.5		0.00728	0.00723		0.00342	0.00340		0.00187	0.00185
7.5		0.00753	0.00745		0.00354	0.00351		0.00193	0.00191
8.5		0.00766	0.00759		0.00363	0.00360		0.00200	0.00198
11.0		0.00810	0.00800		0.00385	0.00380		0.00213	0.00210
13.0		0.00804	0.00791		0.00381	0.00375		0.00212	0.00208
15.0	0.00729	0.00826	0.00811	0.00347	0.00411	0.00386	0.00193	0.00219	0.00215
17.0	0.00727	0.00824	0.00807	0.00349	0.00396	0.00388	0.00155	0.00217	0.00213
19.0	0.00728	0.00823	0.00804	0.00353	0.00399	0.00390	0.00197	0.00223	0.00218
22.5	0.00745	0.00843	0.00819	0.00354	0.00406	0.00395	0.00202	0.00229	0.00222
27.5	0.00747	0.00849	0.00820	0.00359	0.00403	0.00389	0.00206	[illegible]	[illegible]
32.5	0.00735	0.00839	0.00808	0.00362	0.00414	0.00398	0.00199	0.00227	0.00219
37.5	0.00723	0.00831	0.00795	0.00358	0.00411	0.00394	0.00204	0.00234	0.00224
42.5	0.00750	0.00867	0.00823	0.00361	0.00417	0.00396	0.00203	0.00235	0.00223

*$B(\mu r) = 1 + 0.7(\mu r)^{0.72}$ $\mu = \mu_T = 1/445$ ft.

†$B(\mu r) = 1$ $\mu = \mu_T = 1/445$ ft.

‡$B(\mu r) = 1$ $\mu = \mu_A = 1/947.2$ ft.

TABLE 12

ASYMPTOTIC SCATTERING FUNCTION AND INFINITE FIELD DOSE RATE
CYLINDRICAL STRUCTURES

Depth (in.)	D(r = 45)	Δg_s^1	D_1^*	Δg_s^2	D_2^*	Δg_s^3	D_3^*	ω_u'
				1/2-in. Cylinder				
1.00	33.75	0.0894	53.48	0.102	50.01	0.095	54.77	0.917
2.00	28.69	0.0766	45.83	0.088	42.72	0.084	47.50	0.836
2.75	24.44	0.0682	39.49	0.078	36.87	0.073	40.59	0.776
3.00	23.98	0.0638	38.06	0.072	35.46	0.068	39.03	0.757
4.25	19.16	0.0546	31.21	0.0613	28.93	0.059	32.22	0.666
4.5	19.27	0.0524	30.83	0.060	28.83	0.058	32.11	0.649
5.75	15.30	0.0434	24.88	0.0504	23.33	0.047	25.70	0.568
6.00	15.15	0.0417	24.35	0.0475	22.72	0.044	24.89	0.553
8.75	10.13	0.0299	16.73	0.0335	15.47	0.0325	17.32	0.410
11.75	7.03	0.0214	11.75	0.0239	10.84	0.0230	12.12	0.286
17.75	3.76	0.0119	6.39	0.0136	5.92	0.0130	6.64	0.171
23.75	2.28	0.00740	3.91	0.00838	3.62	0.00810	4.07	0.107
35.75	1.057	0.00359	1.85	0.00404	1.699	0.00395	1.929	0.052
47.75	0.579	0.00202	1.025	0.00229	0.944	0.00225	1.074	0.030
				1-in. Cylinder				
1.00	33.61	0.0937	54.29	0.0980	49.20	0.094	54.41	
2.00	27.67	0.0761	44.47	0.0850	41.22	0.081	45.60	
2.75	26.05	0.0698	41.45	0.0776	38.42	0.075	42.65	
3.00	23.48	0.0639	37.58	0.0670	34.16	0.065	37.86	
4.25	20.73	0.0565	33.20	0.0632	30.80	0.062	34.45	
4.5	18.24	0.0511	29.52	0.0530	26.69	0.052	29.75	
5.75	15.91	0.0438	25.58	0.0484	23.62	0.045	25.87	
6.00	14.68	0.0423	24.02	0.0440	21.69	0.0405	23.64	
8.75	9.983	0.0276	16.07	0.0311	14.94	0.0300	16.62	
11.75	6.527	0.0189	10.70	0.0212	9.906	0.0205	11.06	
17.75	3.281	0.0108	5.665	0.01205	5.202	0.0118	5.892	
23.75	1.883	0.00612	3.234	0.00692	2.986	0.0065	3.321	
35.75	0.839	0.. 287	1.472	0.00316	1.343	0.00305	1.514	
47.75	0.453	0.00154	0.7929	0.00173	0.7288	0.0017	0.8292	
				1-1/2-in. Cylinder				
1.00	29.67	0.0749	46.20	0.082	42.74	0.087	48.92	
2.00	24.52	0.0632	38.47	0.072	36.00	0.067	39.35	
2.75	21.76	0.0565	34.23	0.0610	31.48	0.058	34.60	
3.00	21.09	0.0562	33.49	0.060	30.65	0.057	33.70	
4.25	16.40	0.0431	25.91	0.048	24.05	0.045	26.36	
4.5	16.64	0.0429	26.11	0.047	24.12	0.044	26.38	
5.75	12.46	0.0336	19.88	0.0375	18.44	0.035	20.21	
6.00	13.02	0.0352	20.79	0.037	18.92	0.034	20.54	
8.75	7.623	0.0210	12.26	0.023	11.29	0.022	12.49	
11.75	4.660	0.0138	7.706	0.0155	7.131	0.015	7.979	
17.75	2.267	0.00701	3.814	0.00795	3.534	0.0075	3.927	
23.75	1.302	0.00420	2.229	0.0046	2.035	0.0045	2.298	
35.75	0.5785	0.00197	1.013	0.00225	0.9372	0.0022	1.065	
47.75	0.3102	0.00105	0.5419	0.00120	0.5015	0.00115	0.5647	

TABLE 12 (Cont'd.)

ASYMPTOTIC SCATTERING FUNCTION AND INFINITE FIELD DOSE RATE
CYLINDRICAL STRUCTURES

Depth (in.)	D(r = 45)	Δg_s^1	D_1^∞	Δg_s^2	D_2^∞	Δg_s^3	D_3^∞
			2-in. Cylinder				
1.00	21.70	0.0557	33.55	0.059	30.95	0.056	34.09
2.00	18.42	0.0456	28.48	0.050	26.39	0.048	29.04
2.75	16.04	0.0421	25.33	0.047	23.53	0.044	25.78
3.00	15.60	0.0384	24.07	0.045	22.77	0.042	24.89
4.25	11.89	0.0317	18.89	0.036	17.63	0.034	19.41
4.5	11.78	0.0295	18.29	0.035	17.26	0.032	18.86
5.75	9.106	0.0246	14.54	0.028	13.57	0.028	15.30
6.00	9.454	0.0253	15.04	0.028	13.92	0.0265	15.32
8.75	5.214	0.0149	8.502	0.017	7.924	0.016	8.755
11.75	3.222	0.00959	5.339	0.0109	4.959	0.0105	5.546
17.75	1.506	0.00473	2.554	0.0054	2.367	0.0052	2.657
23.75	0.8525	0.00274	1.457	0.0031	1.347	0.00295	1.505
35.75	0.3722	0.00126	0.6503	0.0014	0.5954	0.00135	0.6710
47.75	0.2141	0.000787	0.3878	0.00091	0.3592	0.00087	0.4066

TABLE 13

INFINITE FIELD DOSE RATES
RECTANGULAR STRUCTURE

Depth (in.)	D_1^∞
1.0	36.98
2.0	26.12
3.0	18.52
4.0	14.65
6.0	9.27
12.0	3.803
24.0	1.716
36.0	0.918

TABLE 14

D^{∞} CALCULATIONS USING THE ENGINEERING MANUAL METHOD*

$\omega_{u'}$	$S_a(\omega_{u'})$	ω_u	$S_a(\omega_u)$	$S_a(\omega_{u'})-S_a(\omega_u)$	D^{∞}/D_o (1/2 in.)	D^{∞}/D_o (1 in.)	D^{∞}/D_o (1 in. rect.)	D^{∞}/D_o (1-1/2 in.)	D^{∞}/D_o (2 in.)
0.917	0.758	0.01880	0.0049	0.7531	0.1516	0.1333		0.0973	0.0685
0.836	0.602	0.01821	0.00475	0.5972	0.1202	0.1057		0.0771	0.0543
0.809	0.565	0.0143	0.00373	0.5613			0.06691		
0.776	0.518	0.01777	0.00464	0.5134	0.1033	0.0909		0.0663	0.0467
0.757	0.488	0.01767	0.00461	0.4834	0.0973	0.0856		0.0624	0.0440
0.670	0.400	0.0139	0.00363	0.3964			0.04725		
0.666	0.388	0.01704	0.00445	0.3835	0.0771	0.0678		0.0495	0.0349
0.649	0.376	0.01686	0.00440	0.3716	0.0747	0.0657		0.0480	0.0338
0.568	0.301	0.01633	0.00426	0.2967	0.0596	0.0525		0.0383	0.0269
0.556	0.290	0.0136	0.00355	0.2865			0.03415		
0.553	0.288	0.01612	0.00421	0.2838	0.0570	0.0502		0.0366	0.0258
0.465	0.225	0.0133	0.00347	0.2215			0.02640		
0.410	0.185	0.01497	0.00391	0.1811	0.0364	0.0320		0.0233	0.0164
0.340	0.145	0.0125	0.00326	0.1417			0.01689		
0.286	0.122	0.01367	0.00357	0.1184	0.0239	0.0210		0.0153	0.01077
0.171	0.0628	0.01165	0.00304	0.0598	0.01205	0.0106		0.00773	0.00544
0.168	0.0620	0.0112	0.00292	0.0591			0.00704		
0.107	0.0350	0.01007	0.00262	0.0324	0.00653	0.00574		0.00419	0.00295
0.0710	0.0218	0.0086	0.00224	0.0196			0.00234		
0.052	0.0159	0.00767	0.00200	0.0139	0.00280	0.00246		0.00180	0.00126
0.0385	0.0112	0.0071	0.00185	0.00935			0.00111		
0.030	0.0084	0.00610	0.00159	0.00681	0.00137	0.00121		0.000881	0.000620

*Note: $D^{\infty}/D_o = B_w\, 0.5\, S_w\, E\left[S_a(\omega_{u'})-S_a(\omega_u)\right] + 0.088(1-S_w)\left[S_a(\omega_{u'})-S_a(\omega_u)\right]$

Cylinder: $E=\frac{\pi}{2}$ $D^{\infty}/D_o = B_w\,(0.697\,S_w + 0.088)\left[S_a(\omega_{u'})-S_a(\omega_u)\right]$

Rectangular wall: $E=1$ $D^{\infty}/D_o = B_w\,(0.412\,S_w + 0.088)\left[S_a(\omega_{u'})-S_a(\omega_u)\right]$

Wall thickness (in.)	X_c (psf)	B_w	S_w
1/2	18.6	0.62	0.34
1	37.2	0.4	0.51
1-1/2	55.9	0.252	0.61
2	74.5	0.162	0.68

TABLE 15

COMPARISON OF EXPERIMENTAL AND THEORETICAL VALUES OF D^{∞}

ω_u	1/2-in. Cylinder			1-in. Cylinder			1-1/2-in. Cylinder			2-in. Cylinder			1-in. Rectangular		
	$\frac{D^{\infty}_{exp}}{D_o}$ *	$\frac{D^{\infty}_{calc}}{D_o}$	$\frac{D_{exp}}{D_{calc}}$	$\frac{D^{\infty}_{exp}}{D_o}$	$\frac{D^{\infty}_{calc}}{D_o}$	$\frac{D_{exp}}{D_{calc}}$	$\frac{D^{\infty}_{exp}}{D_o}$	$\frac{D^{\infty}_{calc}}{D_o}$	$\frac{D_{exp}}{D_{calc}}$	$\frac{D^{\infty}_{exp}}{D_o}$	$\frac{D^{\infty}_{calc}}{D_o}$	$\frac{D_{exp}}{D_{calc}}$	$\frac{D^{\infty}_{exp}}{D_o}$	$\frac{D^{\infty}_{calc}}{D_o}$	$\frac{D_{exp}}{D_{calc}}$
0.917	0.1076	0.1516	0.710	0.1092	0.1333	0.819	0.0930	0.0973	0.956	0.0675	0.0685	0.985			
0.836	0.0967	0.1202	0.804	0.0895	0.1057	0.847	0.0774	0.0771	1.004	0.0573	0.0543	1.055			
													0.0744	0.0669	1.112
0.776	0.0795	0.1033	0.770	0.0834	0.0909	0.917	0.0689	0.0663	1.039	0.0510	0.0467	1.092			
0.757	0.0766	0.0973	0.787	0.0756	0.0856	0.883	0.0674	0.0624	1.080	0.0484	[illegible]	1.100			
													0.0526	0.0472	1.114
0.666	0.0628	0.0771	0.815	0.0668	0.0678	0.985	0.0521	0.0495	1.053	0.0380	0.0349	1.089			
0.649	0.0620	0.0747	0.830	0.0594	0.0657	0.904	0.0525	0.0480	1.094	0.0368	0.0338	1.089			
0.568	0.0501	0.0596	0.841	0.0515	0.0525	0.981	0.0400	0.0383	1.044	0.0293	0.0269	1.089			
													0.0373	0.0341	1.094
0.553	0.0490	0.0570	0.860	0.0483	0.0502	0.962	0.0418	0.0366	1.142	0.0303	0.0258	1.174			
													0.0295	0.0264	1.117
0.410	0.0337	0.0364	0.926	0.0323	0.0320	1.009	0.0247	0.0233	1.060	0.01711	0.0164	1.043			
													0.0187	0.0169	1.107
0.286	0.0236	0.0239	0.987	0.0215	0.02098	1.025	0.0155	0.01531	1.012	0.01074	0.01077	0.997			
0.171	0.01286	0.01205	1.067	0.0114	0.01060	1.075	0.00767	0.00773	0.992	0.00514	0.00544	0.945			
													0.00765	0.00704	1.087
0.137	0.00787	[illegible]	1.205	[illegible]	0.00574	[illegible]	0.00448	[illegible]	[illegible]	[illegible]	0.00295	[illegible]			
													0.00345	0.00234	1.474
0.052	0.00372	0.00280	1.329	0.00296	0.00246	1.203	0.00204	0.00180	1.133	0.001308	0.00126	1.038			
													0.00185	0.00111	1.667
0.030	0.00206	0.00137	1.504	0.00160	0.00121	1.322	0.00109	0.000881	1.237	0.00078	0.00062	1.258			

*The D^{∞}_{exp} presented here is equal to the measured dose rate divided by 497 to give a ratio to the dose rate 3 ft above an infinite plane uniformly contaminated with 1 curie/ft^2.

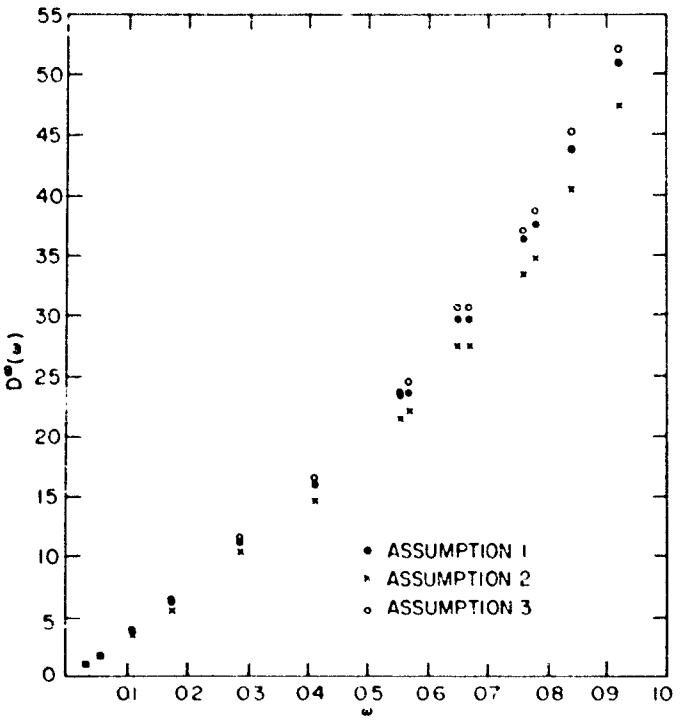

Figure 7. $D^{\infty}(\omega)$ vs ω, 1-in. Thick Cylinder

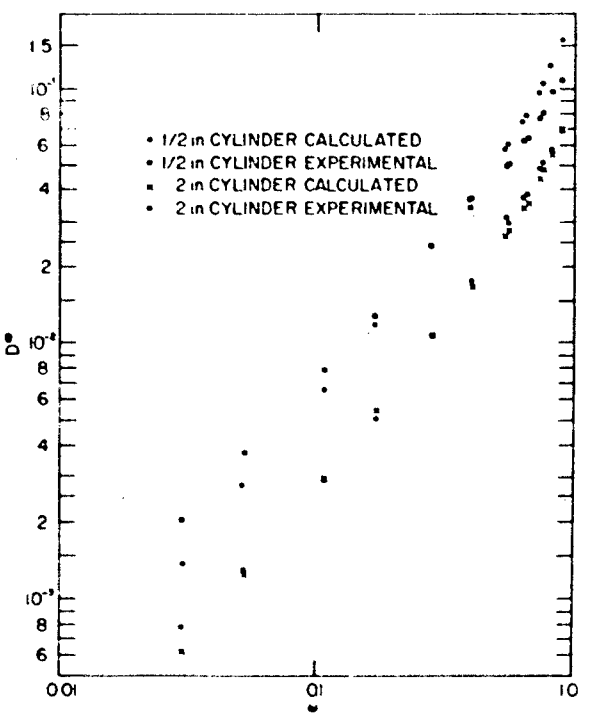

Figure 8. D^{∞} vs ω, Calculated and Experimental Values

CHAPTER 5

RESULTS AND CONCLUSIONS

EXPERIMENTAL ERROR

The opportunities for error lay in the interpretation and extrapolation of the data as well as in the experimental limitations of accuracy. In taking readings, error could arise from

1. Incorrect source position
2. Surface irregularities
3. Incorrect detector position
4. Consistent inaccuracy of the detectors
5. Normal dosimeter spread and reader-charger readout limitations
6. Finite size of detectors.

Calculational errors would be most likely in determining the value of Δg_s from the plots (see Figure 6) and in extrapolating $D^{\infty}(\omega)$ to $\omega = 1$.

Most of the experimental errors can be considered more or less statistical fluctuations because of the large number of independent positionings and readings that went into the final values of D^{∞}. For the dosimeters this is true of 1, 3, and 5 above; for the ratemeter, which was left undisturbed while a radial series of points was measured, 3 could have been serious if accurate positioning of the ratemeter had not been ensured. Surface irregularities were recognized and compensated for. Since the same dosimeters were consistently used in the same positions, sizable differences in individual responses would distort the final result. However, these differences did not exceed 2 to 3% in subsequent measurements. The ratemeter, for which 6 might be significant, was used only at the greater depths where the flux changed reasonably slowly.

Scatter of individual measurements showed up strongly in the plot of Δg_s vs radius in Figure 6 to give a somewhat uncertain asymptotic value. Hopefully, the use of three approaches, calculated from the Δg_s curves on different days in different

moods, leads to some statistical reduction of error in the average value. The variation of the quadratic fitted to the $D^{\infty}(\omega)$ points from those points was no more than 2% at the larger values of ω. There could be up to 4% error in the treatment of air-scattered radiation. On the basis of these considerations, the data should be accurate to within 10%.

COMPARISON OF EXPERIMENTAL AND THEORETICAL RESULTS

As shown in Table 15 there is good agreement between theory and experiment for all but the thinnest wall and largest solid angle. In thin walls, of course, the assumption breaks down that multiple scattering will mask the difference in response to various parts of the wall.

The $G_s(\omega)$ curve rests on the assumption that equal increments of solid angle will give equal response no matter what the height of the angles above the source plane or equivalently the detector position below the plane. But in reality the expression

$$D^{\infty} = 0.5\,\alpha\left[S_a(\omega_{u'}) - S_a(\omega_u)\right]$$

is valid only for a detector position at the level of the source plane in a semi-infinite cylinder; i.e.,

$$D^{\infty}(\omega_{u'} = 1) = 0.5\,\alpha\left[1 - 0\right] = 0.5\,\alpha.$$

For positions below the surface, the correct expression would be

$$D^{\infty}(\omega_{u'}) = 0.5\,f(d)\alpha\left[S_a(\omega_{u'}) - S_a(\omega_u)\right], \qquad (16)$$

with $f(d) > 1$, since lowering the detector is equivalent to raising the source plane thus putting it closer to each incremental scattering area that is still exposed. This form, of course, is necessitated by the retention of the theoretical $S_a(\omega)$ rather than by adopting a new, experimental form. The theoretical value would be expected to have sufficient generality to justify modification rather than replacement. In Chapter 6 the experimental curves are found to tend toward Spencer's as a limiting value.

This leads to two conclusions about the terms of Eq. (11):

1. The values of the components of $\left[0.5 S_w B_w E + 0.088 B_w (1 - S_w)\right]$ may be wrong since the theoretical expression should be quite accurate for $\omega_{u'} \approx 1$. Then if the composite value is changed to agree with an extrapolated experimental value of D^{∞} at $\omega = 1$, a new set of calculated values for $D(\omega)$ is obtained as shown in Table 16. A comparison of α_{exp} with the theoretical expression is shown in Table 17.

2. For each measured value of ω, f(d) can then be determined, assuming $S_a(\omega, d)$ actually represents wall-scattered radiation and the wall-scattered and air-scattered (0.5 and 0.088) components vary identically with depth. Table 16 also shows f(d).

CONCLUSIONS

Agreement within about 20% is found for most of the positions and wall thicknesses, except the thinnest, for which the greatest discrepancy would be expected.

If the validity of $S_a(d, \omega)$ is accepted and the barrier factors are questioned, a different value for $\left[0.5 S_w B_w E + 0.088 B_w (1 - S_w)\right]$ is found from the known behavior of S_a at $\omega = 1$ and the extrapolated value of D^{∞}. The factor $S_a(\omega)$ is defined as equal to 1 at $\omega = 1$ and as equal to 0 at $\omega = 0$. Therefore, theory requires that a detector at the intersection of a semi-infinite cylinder with a plane of radiation, subtending lower solid angle $\omega_{u'} = 1$ and upper angle $\omega_u = 0$, receives dose rate

$$D^{\infty} = \alpha \left[S_a(1) - S_a(0)\right] = \alpha.$$

Thus an experimental value for B_w $\left[0.5 S_w E + 0.088(1 - S_w)\right]$ could be found, except for the finite size of the cylinder and detector. The missing portion of the cylinder between 5 ft and infinity represents a very small part of the dose rate at the higher detector positions and can be adequately approximated by its theoretical value, $\alpha S_a(\omega_u)$.

TABLE 16

D^{∞} CALCULATED FROM EXTRAPOLATED VALUES OF D^{∞}_{exp} TO DETERMINE f(d)*

$\omega_{u'}$	$\frac{D^{\infty}_{calc}}{D_o}$	$\frac{D^{\infty}_{exp}}{D_o}$	f(d)	$\frac{D^{\infty}_{calc}}{D_o}$	$\frac{D^{\infty}_{exp}}{D_o}$	f(d)
	1/2-in. Cylinder[1]			1-in. Cylinder[2]		
0.917	0.0947	0.1076	1.136	0.0943	0.1092	1.158
0.836	0.0751	0.0917	1.221	0.0748	0.0895	1.196
0.776	0.0650	0.0795	1.223	0.0647	0.0834	1.289
0.757	0.0598	0.0766	1.281	0.0595	0.0756	1.270
0.666	0.0482	0.0628	1.303	0.0480	0.0668	1.392
0.649	0.0467	0.0620	1.328	0.0465	0.0594	1.278
0.568	0.0373	0.0501	1.343	0.0371	0.0515	1.388
0.553	0.0357	0.0490	1.373	0.0356	0.0483	1.358
0.410	0.0228	0.0337	1.478	0.0227	0.0323	1.424
0.286	0.0149	0.0236	1.584	0.0148	0.0215	1.450
0.171	0.00752	0.01286	1.710	0.00749	0.0114	1.522
0.107	0.00407	0.00787	1.934	0.00406	0.00651	1.604
0.052	0.00175	0.00372	2.126	0.00174	0.00296	1.697
0.030	0.000856	0.00206	2.407	0.000853	0.00160	1.876

*Note: $D^{\infty}(\omega) = B_w\left[0.5 S_w E + 0.088(1 - S_w)\right]\left[S_a(\omega_{u'}) - S_a(\omega_u)\right] = \alpha\left[S_a(\omega_{u'}) - S_a(\omega_u)\right]$

$$\alpha = \frac{D^{\infty}(1)}{1 - S_a(\omega_{um})} = \frac{D^{\infty}(1)}{1 - 0.0058} = \frac{D^{\infty}(1)}{0.9942}$$

1. $D^{\infty}(1) = 62.04$ $\alpha = 62.40$ $\frac{\alpha}{497} = 0.1255$

2. $D^{\infty}(1) = 61.87$ $\alpha = 62.23$ $\frac{\alpha}{497} = 0.1252$

TABLE 16 (Cont'd.)

D^{∞} CALCULATED FROM EXTRAPOLATED VALUES OF D_{exp} TO DETERMINE f(d)

$\omega_{u'}$	$\frac{D^{\infty}_{calc}}{D_o}$	$\frac{D^{\infty}_{exp}}{D_o}$	f(d)	$\frac{D^{\infty}_{calc}}{D_o}$	$\frac{D^{\infty}_{exp}}{D_o}$	f(d)
	1-1/2-in. Cylinder[3]			2-in. Cylinder[4]		
0.917	0.0812	0.0930	1.146	0.0580	0.0675	1.164
0.836	0.0644	0.0774	1.203	0.0459	0.0573	1.248
0.776	0.0558	0.0689	1.236	0.0398	0.0510	1.283
0.757	0.0513	0.0674	1.315	0.0366	0.0484	1.321
0.666	0.0413	0.0521	1.262	0.0295	0.0380	1.286
0.649	0.0401	0.0525	1.311	0.0286	0.0368	1.286
0.568	0.0320	0.0400	1.251	0.0229	0.0293	1.282
0.553	0.0306	0.0418	1.368	0.0218	0.0303	1.387
0.410	0.0195	0.0247	1.264	0.0139	0.01711	1.228
0.286	0.0127	0.0155	1.216	0.00910	0.01074	1.179
0.171	0.00645	0.00767	1.190	0.00460	0.00514	1.117
0.107	0.00349	0.00448	1.285	0.00249	0.00293	1.176
0.052	0.00149	0.00204	1.366	0.00107	0.001308	1.223
0.030	0.000734	0.00109	1.486	0.000524	0.00078	1.488
	1-in. Rectangular[5]					
0.808	0.0607	0.0744	1.226			
0.670	0.0420	0.0526	1.252			
0.556	0.0307	0.0373	1.215			
0.465	0.0229	0.0295	1.288			
0.340	0.0151	0.0187	1.238			
0.168	0.00602	0.00765	1.271			
0.071	0.00182	0.00345	1.896			
0.0385	0.000984	0.00185	1.880			

3. $D^{\infty}(1) = 53.27$ $\quad \alpha = 53.59$

$\frac{\alpha}{497} = 0.1078$

4. $D^{\infty}(1) = 38.01$ $\quad \alpha = 38.23$

$\frac{\alpha}{497} = 0.07692$

5. $D^{\infty}(1) = 55.05$ $\quad \alpha = \frac{D^{\infty}(1)}{1 - 0.0042} = \frac{D^{\infty}(1)}{0.9958} = 55.28$

$\frac{\alpha}{497} = 0.1112$

TABLE 17

$\left[0.5 S_w B_w E + 0.088 B_w (1 - S_w)\right]$: EXPERIMENTAL AND THEORETICAL VALUES

X_e (psf)	α_{exp}		$\alpha_{theor.}$	$\frac{\alpha_{exp}}{\alpha_{theor.}}$
	Analytic	Visual		
18.6	0.1255	0.132	0.201	0.624
37.2	0.1252	0.135	0.177	0.707
37.2 (rect.)	0.1112		0.119	0.934
55.9	0.1078	0.113	0.129	0.836
74.5	0.0769	0.080	0.091	0.845

Because of the danger of direct beam contribution, the highest detector was an inch below the surface, subtending a solid angle $\omega_{u'} = 0.917$. This is sufficiently close to $\omega_{u'} = 1$ to permit extrapolation of the dose rate to that valuc by visual extension of the $D^{\infty}(\omega)$ vs ω curve or by analytic curve fitting representing D^{∞} by a quadratic in ω determined by the method of least squares. These curves are compared with the data in Table 18. The results of the two methods are compared with the theoretical value in Table 17. A new set of calculated values of D^{∞} is obtained that at least converges toward the experimental value at $\omega = 1$, where agreement would theoretically be inevitable, though the discrepancy at greater depths is now larger. Values of f(d) for each thickness are found to form a fairly smooth family of curves (Figure 9). A possibly significant factor that has been neglected is the variation of $S_a(d, \omega)$ and S(d) with depth or detector distance from the standard height of 3 ft. An attempt to estimate this has been included in Chapter 6.

General agreement has, therefore, been found between the results of this experiment and calculations made using the method and curves of the Engineering Manual. However, significant discrepancies exist that can be accounted for theoretically by assuming that one or all of the factors B_w, S_w, and E are incorrect and that there is an additional factor, f(d) that varies with detector position and wall thickness.

TABLE 18

$D^{\infty}(\omega = 1)$ THROUGH ANALYTIC APPROXIMATION OF $D^{\infty}(\omega)$

ω	1/2 in.		1 in.		1-1/2 in.		2 in.	
	D^{∞}_{anal} [1]	D^{∞}_{exp}	D^{∞}_{anal} [2]	D^{∞}_{exp}	D^{∞}_{anal} [3]	D^{∞}_{exp}	D^{∞}_{anal} [4]	D^{∞}_{exp}
0.917	53.25	53.48	53.40	54.29	45.84	46.20	33.07	33.55
0.836	45.41	45.60	45.76	44.47	39.11	38.47	28.48	28.48
0.776	40.10	39.49	40.50	41.45	34.45	34.23	25.23	25.33
0.757	38.50	38.06	38.92	37.58	33.04	33.49	24.22	24.07
0.666	31.48	31.21	31.92	33.20	26.70	25.91	19.60	18.89
0.649	30.22	30.83	30.55	29.52	25.56	26.11	18.77	18.29
0.568	24.94	24.88	25.05	25.58	20.59	19.88	14.94	14.54
0.553	24.03	24.35	24.09	24.02	19.72	20.79	14.26	15.04
0.410	16.71	16.73	16.05	16.07	12.34	12.26	8.14	8.50

1. $D^{\infty}_{anal} = 8.88 - 4.50\,\omega + 57.70\,\omega^2$
2. $D^{\infty}_{anal} = 4.06 + 9.45\,\omega + 48.36\,\omega^2$
3. $D^{\infty}_{anal} = 0.27 + 13.07\,\omega + 39.93\,\omega^2$
4. $D^{\infty}_{anal} = -5.40 + 25.81\,\omega + 17.60\,\omega^2$

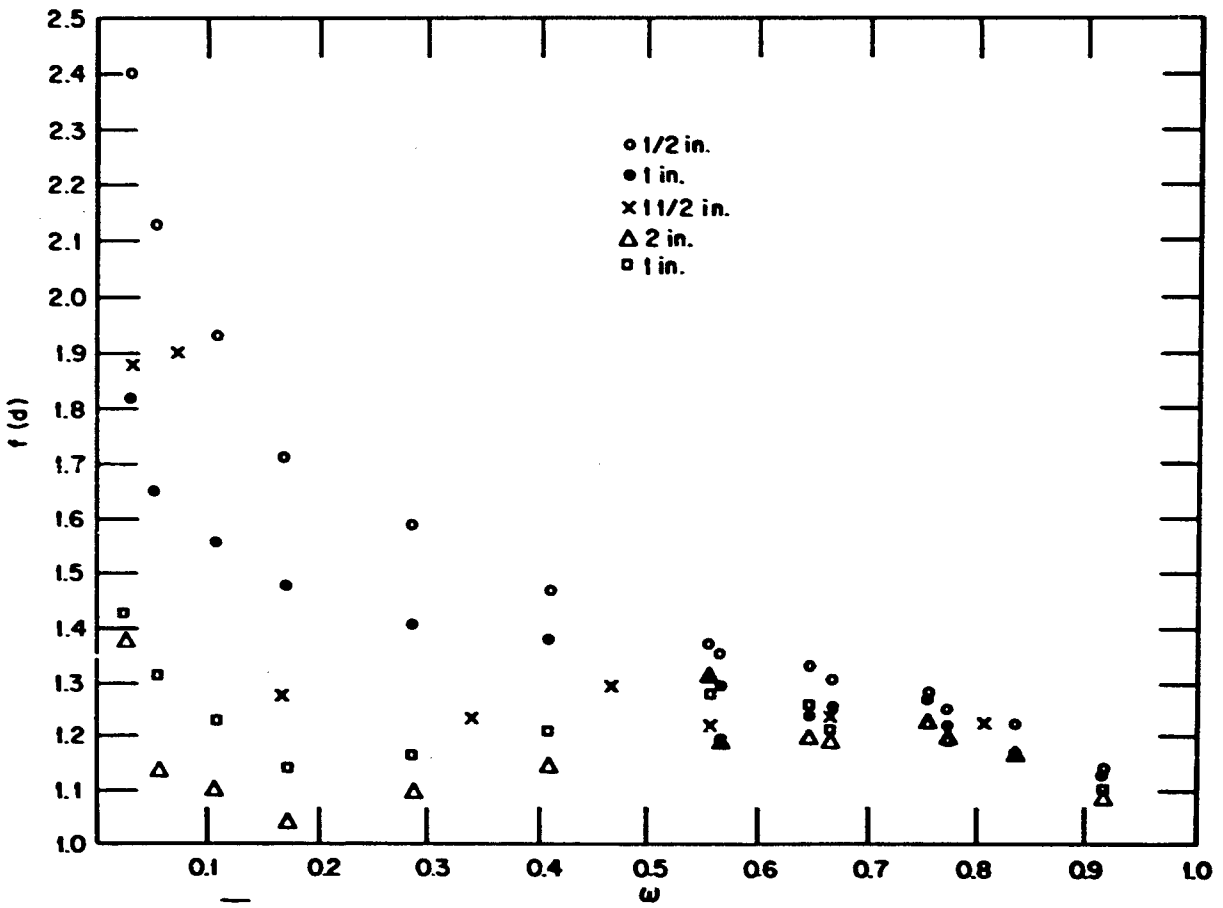

Figure 9. f(d) vs ω

CHAPTER 6

$S_a(\omega)$: DERIVATION OF AN EXPERIMENTAL CURVE

The infinite field dose rate has been found for positions below ground in a steel cylinder and behind a rectangular wall. These values have been compared with those predicted by the method of the Engineering Manual using the expression

$$\frac{D^{\infty}}{D_o} = \alpha \left[S_a(\omega_{u'}) - S_a(\omega_u) \right].$$

The factors $B_w \left[0.5 S_w E + 0.088(1 - S_w) \right]$ are represented by α and can be determined either by using curves given in the Manual or by extrapolating D^{∞} to its value at $\omega = 1$ (see p. 45).

Since the object of this experiment is to evaluate the calculated curve $G_s(\omega)$ or the equivalent $S_a(\omega)$, it is desirable to eliminate the additional variables B_w, S_w, and E by following the second course mentioned above. This experimental value of α can then be used to find an experimental set of values of $S_a(\omega)$ through the equation

$$S_a(\omega_{u'}) = \frac{\frac{D^{\infty}}{D_o}(\omega_{u'}, \omega_u)}{\alpha} + S_a(\omega_u) \qquad (17)$$

if $S_a(\omega_u)$ can somehow be evaluated.

For all values of $\omega_{u'}$ encountered in the experiment, ω_u is small and so is the correction term $S_a(\omega_u)$ (corresponding to the difference between the experimental structure and an ideal, infinite one). Further, this range of $S_a(\omega)$ can be closely approximated by a straight line; i.e., $S_a(\omega_u) = b\omega_u$. Thus a simpler formula can be found with negligible introduction of error

$$S_a(\omega_{u'}) = \frac{\frac{D^{\infty}}{D_o}(\omega_{u'}, \omega_u)}{\alpha} + b\omega_u. \qquad (18)$$

The problem is now reduced to evaluating b. If we return to the original form

$$\frac{D^{\infty}}{D_o}(\omega_{u'}, \omega_u) = \alpha \left[S_a(\omega_{u'}) - S_a(\omega_u) \right]$$

$$= \alpha \left[S_a(\omega_{u'}) - b\omega_u \right] \tag{19}$$

and differentiate, we find

$$\frac{dD^{\infty}}{d\omega_u} = - \alpha b \tag{20}$$

since $S_a(\omega_{u'})$ is independent of ω_u. From the variation in dose rate, $dD^{\infty}/d\omega_u$ can be found with a change in the height of the cylinder, corresponding to a change in ω_u. At a given detector position, the height of the cylinder was increased in steps from 1 to 7 ft, and measurements were made with the source at three radial positions, using the 1/2-in. cylinder. By dividing the change in dose by the accompanying change in solid angle, values for $dD(r)/d\omega_u$ could be found for each radial position. An approximation of $dD^{\infty}/d\omega_u$ could be found by adding the three $dD(r)/d\omega_u \cdot \Delta r$ and a fourth term representing the field from 45 ft to infinity (Table 19). This is obviously a crude approach based on marginal data, but it is justified by the noncriticality of the exact value of b and by the consistency of the value calculated with the derived curve of $S_a(\omega)$.

The theoretical curve of $S_a(\omega)$ used is taken from p. 120 of Spencer's monograph and is based on a constant detector height of 3 ft. Since the experimental variation of ω was achieved by changing the detector height in a structure of constant dimensions, a correction must be made to relate the experimental data to that which would be found at the standard height.

Using Spencer's definition, we find

$$S_a(\omega) = \frac{1}{S(d)} \int_{-1}^{-1+\omega} d(\cos \Theta)\, \ell(d, \cos \Theta).$$

TABLE 19

$\frac{dD(\omega_u', \omega_u)}{d\omega_u}$: EVALUATION OF b

Contribution No.	ΔH \ d(ft)	1-2	2-3	3-4	4-5	5-6	6-7
1	r = 5.25						
	1/4	0.923			2.16		1.29
	1/2	1.067	0.790				2.5
	1	0.951	0.744	0.577			
	2	1.070	0.962	0.517		0.435	
	3	1.154	0.810	0.361		1.25	
	$\left(\frac{dD(r)}{d\omega_u}\right)_{avg}$ = 0.735 Δr = 6.5						
2	r = 9.5						
	1/4	0.521	0.644	0.730		2.39	
	1/2	0.663	0.456	0.270	0.519		
	1	0.622	0.651	0.192	0.344	0.278	
	2	0.698	0.577	0.534	0.250	0.435	
	3	0.673	0.517	0.667	0.130	0.625	
	$\left(\frac{dD(r)}{d\omega_u}\right)_{avg}$ = 0.414 Δr = 13.5						
3	r = 32.5						
	1/4	0.149	0.223		0.562	0.577	
	1/2	0.062	0.182			0.260	
	1	0.163	0.191	0.096	0.172		
	2	0.186	0.096	0.345			
	3	0.183	0.172	0.250		0.437	
	$\left(\frac{dD(r)}{d\omega_u}\right)_{avg}$ = 0.260 Δr = 24						
4	$\frac{dD}{d\omega_u} = \sum \frac{dD(r)}{d\omega_u} \Delta r + 220.7 \frac{d(\Delta g_s)}{d\omega_u}$ $\frac{d(\Delta g_s)}{d\omega_u} = \frac{r}{2\pi q S_o e^{-\mu r} B(\mu r)} \frac{dD(r_{max})}{d\omega_u}$ = 0.3484 · 0.260 = 0.0905						

Note: $\frac{dD}{d\omega_u}$ = 4.797 + 5.589 + 6.240 + 19.973 = 36.60 $b = \frac{1}{\alpha} \frac{dD}{d\omega_u} = \frac{36.60}{62.45} = 0.586$

The total air-scatter received from the upper hemisphere by an isotropic detector at height d is represented by S(d) and will decrease with height symmetrically about the source plane. The integral term gives the fraction of S(d) scattered into the solid angle of the upper limit and, of course, equals S(d) for $\omega = 1$. Since detector positions below ground receive higher dose rates than positions subtending equal solid angle above the source plane, as on p. 45, it can be assumed that Spencer's curve of $\ell(d, \cos\Theta)$ will continue to increase for values of d less than 3 ft. Because the value of ℓ seems to increase with height in the same proportion for all values of cos Θ less than 0, the assumption was made that the integral over ℓ will increase by the same amount. By plotting $\ell(d - 1)$ vs d as given in Spencer's curve (Figure 10), extrapolated values of ℓ for d less than 3 ft could be found and the corresponding values of

$$\int_{-1}^{-1+\omega} d(\cos\Theta)\, \ell(d, \cos\Theta)$$

as shown in Table 20. Again, the inaccuracies of the approach are offset by the smallness of the correction and by the fact that any correction will be an improvement.

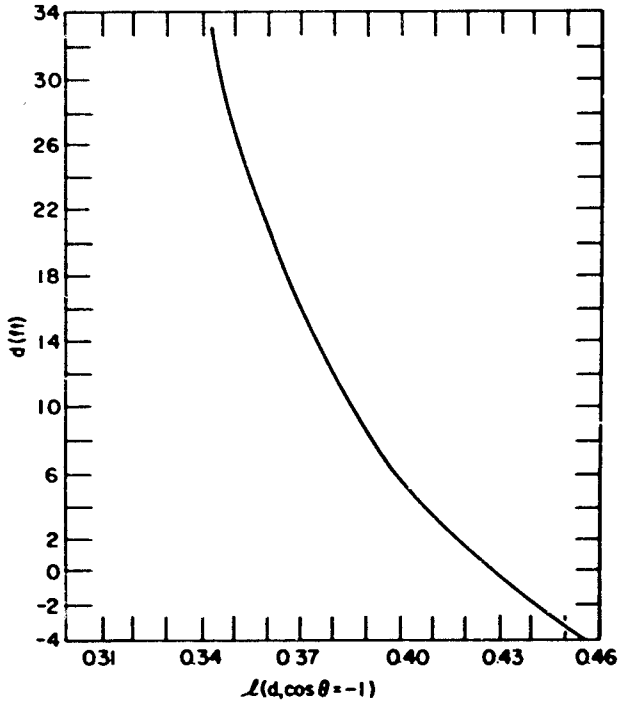

Figure 10. $\ell(d, \cos\Theta = -1)$ vs d

TABLE 20

S(d) and ℓ(d, cos Θ): CORRECTION FACTORS TO FIND D_s^{∞} (3', cos Θ)

$$S_a(3',\omega) = \frac{S(d)}{S(3)} \frac{\lambda(3)}{\lambda(d)} S_a(d,\omega)$$

d (in.)	S(d)	λ(d)	$\frac{S(d)}{S(3')}$	$\frac{\lambda(3')}{\lambda(d)}$	Correction
36	0.0844	0.412	1.00	1.00	–
-1	0.088	0.428	1.043	0.963	1.004
-2	0.088	0.429	1.043	0.960	1.002
-2.75	0.088	0.4295	1.043	0.959	1.001
-3.0	0.088	0.4295	1.043	0.959	1.001
-4.25	0.088	0.43	1.043	0.958	0.999
-4.5	0.088	0.43	1.043	0.958	0.999
-5.75	0.088	0.432	1.043	0.954	0.995
-6.0	0.088	0.432	1.043	0.954	0.995
-8.75	0.088	0.4325	1.043	0.953	0.993
-11.75	0.088	0.434	1.043	0.949	0.990
-17.75	0.0863	0.437	1.023	0.943	0.963
-23.75	0.0850	0.44	1.007	0.936	0.942
-35.75	0.0844	0.448	1.000	0.920	0.920
-47.75	0.0835	0.454	0.989	0.907	0.898

COMPARISON WITH THEORY

Once the experimental values $D^{\infty}(\omega,d)$ have been changed to $D^{\infty}(\omega,3)$, values of $S_a(\omega)$ can be found for each wall thickness (Table 21). The values derived from these data are plotted and are compared with the calculated curve in Figure 11. Curves through these data points are presented in Figure 12. Experiment and theory come into closer agreement as wall thickness increases, indicating that the major cause of the discrepancy lies in the assumption of multiple scattering in the intervening wall to give essentially isotropic scattered radiation. This assumption was made[3] to permit the use of the solid angle subtended by the wall at the detector as

TABLE 21

$S_a(\omega)$: EXPERIMENTAL AND CALCULATED VALUES

ω	1/2 in.	1 in.	1-in. Rect.	1-1/2 in.	2 in.	Calculated
0.917	0.870	0.886		0.877	0.892	0.758
0.836	0.782	0.727		0.730	0.757	0.602
0.808			0.680			0.565
0.776	0.643	0.677		0.650	0.674	0.518
0.757	0.620	0.615		0.636	0.639	0.488
0.670			0.482			0.400
0.656	0.502	0.543		0.492	0.504	0.388
0.649	0.502	0.483		0.496	0.488	0.376
0.568	0.406	0.418		0.379	0.390	0.301
0.556			0.343			0.290
0.553	0.398	0.394		0.395	0.400	0.288
0.465			0.273			0.225
0.410	0.275	0.265		0.236	0.230	0.185
0.340			0.174			0.145
0.286	0.194	0.178		0.150	0.146	0.122
0.171	0.105	0.0945		0.0753	0.0712	0.0628
0.168			0.0745			0.0620
0.107	0.0648	0.0549		0.0450	0.0418	0.0350
0.0710			0.0343			0.0218
0.052	0.0317	0.0262		0.0219	0.0201	0.0159
0.0385			0.0195			0.0112
0.030	0.0183	0.0151		0.0127	0.0127	0.0084

the sole criterion of the radiation scattered to the detector, whether from above or below the detector plane. Obviously, this assumption will be more reasonable in a structure with thicker walls in which multiple scattering will more effectively conceal the different angular distributions of the radiation falling on different sections of the wall.

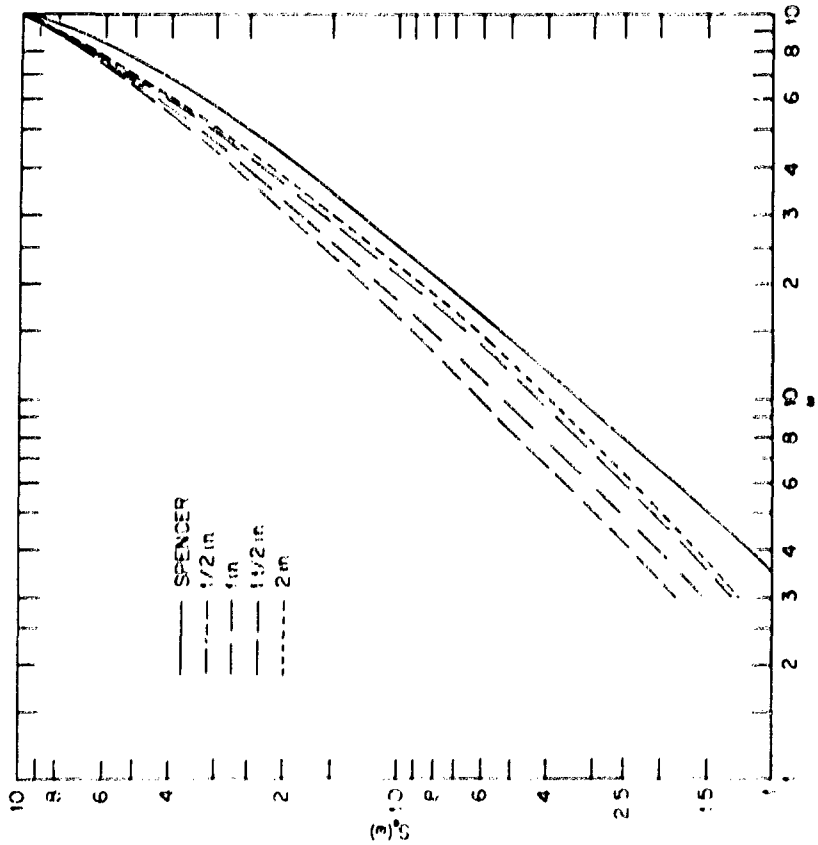

Figure 12. $S_a(\omega)$

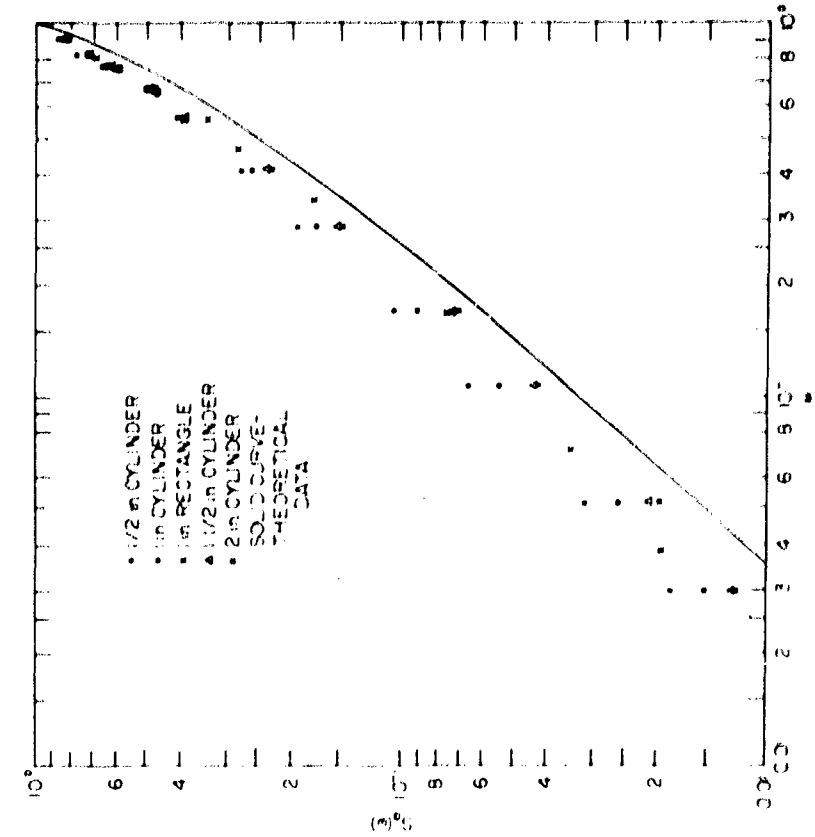

Figure 11. $S_a(\omega)$: Experimental and Theoretical Values

Figure 9, in which f(d) is plotted for each value of X_e, gives an indication of the variation of the scattering properties of the wall with detector positions. This is essentially the same as a ratio of the experimental and calculated values of $S_a(\omega)$ given in Table 21. A series of curves for $S_a(\omega)$ has thus been found that, in the limit of great thickness, approaches that calculated by Spencer. They differ substantially for the smallest solid angles and thinnest walls, though this discrepancy is somewhat offset in dose calculations by a discrepancy in α in the opposite direction. Since experiment predicts a higher dose rate than theory, substantiating experiments would be desirable.

This experiment indicates that the calculational methods of the Engineering Manual are entirely adequate for the evaluation of most shelter situations. However, there does seem to be room for a considerable refinement of theory to interpret the discrepancies encountered.

REFERENCES

1. L. V. Spencer, "Structure Shielding Against Fallout Radiation from Nuclear Weapons," National Bureau of Standards, Monograph 42 (1 June 1962).

2. Office of Civil and Defense Mobilization, "Design and Review of Structures for Protection from Fallout Gamma Radiation" (revised 1 October 1961).

3. C. Eisenhauer, "An Engineering Method for Calculating Protection Afforded by Structures Against Fallout Radiation," National Bureau of Standards Report 7810 (28 February 1963).

4. Personal Communication, Dominic Raso.

5. Best-fit approximation of data from: Rexroad and Schmoke, "Scattered Radiation and Free-Field Dose Rate from Distributed Cobalt-60 and Cesium-137 Sources," NDL-TR-2 (September, 1960) and Batter, "Cobalt and Iridium Buildup Factors Near the Ground-Air Interface," Transactions of the American Nuclear Society 6, 1 (1963), p. 198.

6. "Report of the International Commission on Radiological Units and Measurements," Table 8-1, National Bureau of Standards Handbook 78 (1959).